Effects of 20-100 nanometre particles on liquid clouds in the clean summertime Arctic

W. R. Leaitch, A. Korolev, A. A. Aliabadi
Environment Canada, Toronto, Canada

J. Burkart, M. Willis, J.P.D. Abbatt
Department of Chemistry, University of Toronto, Toronto, Canada

H. Bozem, P. Hoor
Institute of Atmospheric Physics, University of Mainz, Mainz, Germany

F. Köllner, J. Schneider
Particle Chemistry Department, Max Planck Institute for Chemistry, Mainz, Germany

A. Herber, C. Konrad
Alfred Wegener Institute for Polar and Marine Research, Bremerhaven, Germany

R. Brauner
Jade University, Elsfleth, Germany

Date: May 26, 2016

Correspondence to Richard.Leaitch@Canada.ca

Abstract. Observations addressing the effects of aerosol particles on summertime Arctic clouds are scant. An airborne study, carried out during July, 2014 from Resolute Bay, Nunavut, Canada, as part of the Canadian NETCARE project, provides observations enabling a relatively comprehensive in-situ look into some effects of aerosol particles on liquid clouds (fog, stratus and stratocumulus) in the clean environment of the Arctic summer. Sixty-two cloud-averaged data points with the cloud liquid water content (LWC) restricted to ≥ 0.01 g m^{-3} were derived from eight flights. Differences in formation suggest separation between low-altitude (LA) cloud (topped below 200 m: 24 points) and higher-altitude (HA) cloud (based above 200 m: 38 points). Corresponding median LWC and cloud droplet number concentrations (CDNC) are 0.05 g m^{-3} and 10 cm^{-3} for the LA clouds and 0.13 g m^{-3} and 101 cm^{-3} for the HA clouds. The lower activation size of aerosol particles is ≤ 50 nm diameter for about 40% of the points, and the activation of particles as small as 20 nm is suggested for some clouds. Comparisons of the CDNC and cloud condensation nucleus (CCN) concentrations are used to infer average supersaturations (S) of 0.3% and 0.6% for the LA and HA clouds, respectively. Fifteen LA cloud points offer the first observations of aerosol and cloud microphysics within the CCN-limited regime of Mauritsen et al. (2011) in which small increases in CCN are hypothesized to increase LWC and warm the surface. The LWC is found to be positively associated with the CDNC, but there is no association of either the CDNC or LWC with changes in the aerosol. Forty-six points fall in the regime where increased aerosol will more generally cool via the indirect effect, and changes in particles with diameters from 20 nm to 100 nm, which may arise from natural sources, exert a relatively strong influence on the CDNC. A summertime Arctic background CDNC range of 16 cm^{-3} to 160 cm^{-3} (median: 122 cm^{-3}), based on corresponding carbon monoxide below the study median (81 ppbv), offers a reference for the aerosol indirect effect.

1. Introduction

Mass concentrations of the atmospheric aerosol in the Arctic are higher during winter and lower during summer due to differences in transport of anthropogenic particles and wet scavenging (e.g. Barrie, 1986; Stohl, 2006). Much of the focus of atmospheric chemistry and aerosol-cloud research in the Arctic has been on the spring period. That transition from winter to summer offers the opportunity to examine the changes in atmospheric chemistry as the sun rises over the polluted polar atmosphere (e.g. Barrie et al., 1988) and to study the impacts of the anthropogenic aerosol on the Arctic solar radiation balance (e.g. Law and Stohl, 2007; Quinn et al., 2008). Greater-than-expected warming of the Arctic (e.g. Christensen et al., 2013) and rapidly diminishing Arctic sea ice extent (e.g. Maslanik et al., 2011) have drawn considerable attention to the role of anthropogenic and biomass burning aerosols as warming agents for the Arctic (e.g. Law and Stohl, 2007; Quinn et al., 2008; Shindell et al., 2008; Brock et al., 2011; Jacob et al., 2010; UNEP, 2011; Stohl et al., 2013). Recent evidence indicates that the net impact of aerosol particles on the Arctic over the past century has been one of cooling rather than warming (Najafi et al., 2015).

Low-level liquid water clouds are frequent in the sunlit Arctic summer (e.g. Intrieri et al., 2001), and these clouds can have a net cooling effect (e.g. Brenner et al., 2001; Garret et al., 2004; Lubin and Vogelmann, 2010; Zhao and Garrett, 2015; Zamora et al., 2015). Knowledge of the influence of the atmospheric aerosol on climatic aspects of these clouds is complicated by the relatively large potential differences in the albedo of the underlying surface (e.g. Herman, 1977; Lubin and Vogelmann, 2010) and the fact that the Arctic is relatively free of anthropogenic influence in summer, which means that aerosols from natural sources are potentially the most significant sources of nuclei for cloud droplets. Natural sources lead to a shift of the number distribution towards particles smaller than 100 nm (e.g. Heintzenberg and Leck, 1994; Ström et al., 2003; Heintzenberg et al., 2006; Engvall et al., 2008; Tunved et al., 2013; Leaitch et al., 2013; Heintzenberg et al., 2015). Particles much smaller than 100 nm are sometimes dismissed as being too small to nucleate cloud droplets due to the assumption that the cooling mechanisms are too slow to generate the supersaturations (S) required to activate those particles in Arctic liquid clouds (e.g. Garret et al., 2004; Lubin and Vogelmann, 2010; Browse et al., 2014; Zhao and Garrett, 2015). That assumption may result in reduced estimates from natural feedbacks to climate and increased estimates of aerosol indirect forcing from anthropogenic sources.

Lohmann and Leck (2005) hypothesized the need for highly surface-active particles to explain CCN active at S less than 0.3%. However, the cloud S is also strongly constrained by the concentrations of particles larger than 100 nm, and in the clean environment of the summertime Arctic with relatively low concentrations of particles above 100 nm, there is some evidence that higher S may be achieved and smaller particles activated (e.g. Hudson et al., 2010; Korhonen et al., 2010; Leaitch et al., 2013). Further, the suggestion that the minima between 50 nm and 100 nm in summertime Arctic particle size distributions results from cloud processing implies consistent activation sizes much less than 100 nm (Heintzenberg et al., 2015). The effect of the background aerosol on liquid clouds has been identified as one of the most important factors for reducing uncertainty in the aerosol cloud albedo effect (Carslaw et al., 2013), and the effectiveness of particles smaller than 100 nm at nucleating cloud droplets represents a significant part in that uncertainty.

Effects of pollution on clouds may also lead to warming (e.g. Garrett et al., 2009). Mauritsen et al. (2011) modeled cloud radiative forcing for low clouds using CCN number concentrations derived from shipborne observations made over the Arctic Ocean (Tjernström et al., 2004; Tjernström et al., 2014). They found that the impact from changes in CCN for ultra-low values (< 10 cm^{-3}), where CCN concentrations are equivalent to the CDNC in the model, will result in a net warming due to associated longwave changes. Above CCN concentrations of 10 cm^{-3}, increases in CCN are estimated to produce a net cooling of the atmosphere. The threshold CCN concentration is referred to here as the "Mauritsen limit", and it is noted that the value of 10 cm^{-3} is not universal (Mauritsen et al., 2011). In such clean environments, knowledge of the natural aerosol and its influence on the microphysics of summer clouds is critical to the assessment of aerosol effects on Arctic climate.

Past studies of Arctic aerosols and clouds have emphasized the areas of the Beaufort and Chukchi Seas (e.g. Hobbs and Rango, 1998; Curry et al., 2001 and references therein; Lohmann et al., 2001; Peng et al., 2002; Earle et al., 2011; Lance et al., 2011; Jouan et al., 2014; Klingebiel et al., 2014). Most of those studies have focused on the spring when the aerosol can be influenced by anthropogenic or biomass burning aerosols. As well, there has been considerable interest in mixed-phase clouds in the lower Arctic troposphere (e.g. Shupe et al., 2004; Sandvik et al., 2007; Morrison et al., 2012), but a notable lack of in-situ observations of aerosols in combination with liquid water clouds over the Arctic during summer. Among the studies that have considered in-situ measurements of aerosols and Arctic summer clouds, Zamora et al. (2015) examined the efficiency of biomass burning (BB) plumes on indirect forcing, estimating a forcing from these plumes about half of the possible maximum, mostly due to the reduction in cloud-base S by higher concentrations of larger particles that control water uptake. Shupe et al. (2013) discussed some differences among clouds coupled to the surface versus those uncoupled, but did not conduct in-situ observations of the cloud microphysics, and vertical aerosol characterization was constrained to particles >300 nm. Hobbs and Rango (1998) found that low clouds over the Beaufort Sea in June occasionally contained drops as large as 35 μm diameter. They also found that the CDNC in the cloud tops correlated significantly with "aerosols" below the bases. They suggested that cloud-top entrainment did not control the CDNC, although there may be times when entrainment does influence the Arctic CDNC (e.g. Klingebiel et al., 2014).

Motivated by the limited knowledge of aerosol effects on cloud in the summer Arctic and the details of particle activation, the Canadian Network on Climate and Aerosols: Addressing Key Uncertainties in Remote Canadian Environments (NETCARE - http://www.netcare-project.ca/), conducted airborne observations of aerosols and clouds during July, 2014 in the area around Resolute Bay, Nunavut, Canada. The observations from the study are used here to characterize CDNC, LWC, and the volume-weighted mean droplet diameter (VMD). Further, aerosol particle size distributions (5 nm and larger) and CCN from outside of clouds are compared with CDNC to address the following questions:

1) Given the scarcity of data, what are the characteristics of clouds in the summertime Arctic, and do clouds near the surface have characteristics different from those aloft? (Sect. 3.1 and 3.2)
2) What are the sizes of particles that act as nuclei for cloud droplets? Will this enable a closer connection to be made between aerosol processes, particle sizes and climate effects? (Sect. 3.3)
3) What is the relationship between droplet size and droplet number? In particular, what is the aerosol influence on cloud below the Mauritsen-limit, and is it possible to assess a background influence of the aerosol on clouds in the Arctic summer? (Sect. 3.4)

2. Methodologies

The instrument platform was the Alfred Wegener Institute (AWI) Polar 6 aircraft, a DC-3 aircraft converted to a Basler BT-67 (see Herber, A., Dethloff, K., Haas, C., Steinhage, D., Strapp, J. W., Bottenheim, J., McElroy, T. and Yamanouchi, T.; POLAR 5 - a new research aircraft for improved access to the Arctic, ISAR-1, Drastic Change under the Global Warming, Extended Abstract, pp. 54-57, 2008).

2.1 Instrumentation

The following outlines the measurements are relevant to this discussion. Details of the instrument calibrations and evaluations are given in the Supplement (S1).

a) Particle number concentrations >5 nm diameter were measured with a TSI 3787 water-based ultrafine condensation particle counter (UCPC), sampling at a flow rate of 0.6 L min^{-1}. Hereafter, the measurements are referred to as N5.
b) Aerosol particle size distributions from 20 nm to 100 nm (45 s up scans and 15 s down scans) were measured using a Brechtel Manufacturing Incorporated (BMI) Scanning Mobility System (SMS) coupled with a TSI 3010 Condensation Particle Counter (CPC). The sheath and sample flows were set to 6 L min^{-1} and 1 L min^{-1}. BMI software was used to process the distributions.

c) Aerosol particle size distributions from 70 nm to 1 μm were measured using a Droplet Measurement Technology (DMT) Ultra High Sensitivity Aerosol Spectrometer (UHSAS) that uses scattering of 1054 nm laser light to detect particles (e.g. Cai et al., 2008).

d) CCNC(0.6%) were measured using a DMT CCN Model 100 counter operating behind a DMT low pressure inlet at a reduced pressure of approximately 650 hPa. For the nominal water S of 1%, the effective S at 650 hPa was found to be 0.6%. The S was held constant throughout the study to allow for more stability of measurement, improved response, and to examine the hygroscopicity of smaller particles.

e) Droplet size distributions from 2-45 μm were measured using a Particle Measuring Systems (PMS) FSSP-100. This FSSP-100 had been modified with new tips to reduce shattering artifacts (Korolev et al., 2011), and it was mounted in a canister under the port-side wing. The CDNC, VMD and LWC are calculated from the measured droplet distributions.

f) Cloud particle images in two dimensions for particles sized from about 50 μm to 800 μm were measured using a PMS 2DC Grey-scale probe. For the present study, these observations are used only to ensure the absence of the ice phase. This 2DC-Grey was also modified with new tips to reduce shattering artifacts (Korolev et al., 2011), and it was mounted in a canister beside the FSSP-100.

g) Carbon monoxide (CO) is used here as a relative indicator of aerosol influenced by pollution sources and as a potential tracer for aerosol particles entering cloud. The CO was measured with an Aerolaser ultra-fast carbon monoxide monitor model AL 5002 based on VUV-fluorimetry, employing the excitation of CO at 150nm. The instrument was modified such that in-situ calibrations could be conducted in flight.

2.1 State parameters and Winds

State parameters and meteorological measurements were measured with an AIMMS-20, manufactured by Aventech Research Inc. The instrument consists of three modules: 1) an Air Data Probe that measures the three-dimensional aircraft-relative flow vector (true air speed, angle-of-attack, and sideslip), temperature and relative humidity, and includes a three-axis accelerometer pack for turbulence measurement; 2) an Inertial Measurement Unit that consists of three gyros and three accelerometers providing the aircraft angular rate and acceleration; 3) a Global Positioning System for aircraft 3D position and inertial velocity. Horizontal and vertical wind speeds are measured with accuracies of 0.50 and 0.75 m/s, respectively; the vertical resolution was insufficient to measure gusts in the sampled clouds. The accuracy and resolution for temperature measurement are 0.30 and 0.01 C. The accuracy and resolution for relative humidity measurement are 2.0 and 0.1 %. The sampling frequency is 1 Hz.

2.2 Inlets

Aerosol particles were sampled through a shrouded diffuser inlet (diameter of 0.35 cm at intake point), which had been evaluated for larger particle transmission by Leaitch et al. (2010). For the airspeeds during this study, transmission of particles by the inlet is approximately unity for particles from 20 nm to <1 µm. The intake was connected inside the cabin to a 1.9 cm OD stainless steel manifold off of which sample lines were drawn to the various instrument racks using angled inserts. The total flow at the intake point was approximately isokinetic at 55 L min^{-1} based on the sum of flows drawn by the instrumentation (35 L min^{-1}) and the measured flow at the exhaust of the tube. The flow at the exhaust of the tube was allowed to flow freely into the back of the cabin so that the flow at the intake varied by the aircraft TAS and the manifold was not significantly over pressured.

CO was sampled through a separate inlet consisting of a 0.40 cm OD Teflon tube using the forward motion of the aircraft to push air into the line in combination with a rear-facing 0.95 cm OD Teflon exhaust line that lowered the line pressure. The continuously measured sample flow was approximately 12 L min^{-1}.

2.3 Approach to Analysis

Eleven research flights were conducted from Resolute Bay, Nunavut (74°40'48"N 94°52'12"W) beginning July 4 and ending July 21, 2014. The measurements were associated with two relatively distinct weather regimes. During period 1 (July 4-12), the weather conditions around Resolute Bay were affected by an upper low (Supplement Fig. S4). The wind speeds at 500 hPa were mostly calm and varying from south to north. The surface (1000 hPa) was dominated by weak high-pressure with generally clear skies, light winds, and occasional scattered to broken stratocumulus. Low-cloud or fog was at times present in association with open water, and the air was relatively clean as discussed below. There was a transition period from July 13-16 when flights were not possible due to fog at Resolute Bay. During period 2 (July 17-21), the area came under the influence of a deep low pressure system to the south (Supplement Fig. S5) accompanied by more wind and higher cloud. The air was not as clean as during period 1, based on the measured aerosol mass and CO concentrations (see Table 1), possibly due in part to transport of BB aerosol from the Northwest Territories; see further discussion in Section 2.3.1. Using the method of bulk Richardson number and a critical bulk Richardson number of 0.5 with data from radiosondes, Aliabadi et al. (2016a,b) estimated boundary-layer heights at 275 m (±164 m) during the study.

A summary of all flight tracks is shown in Fig. 1. Flights mostly consisted of vertical profiles and of low level flying over ice, water and melt ponds that contributed to the formation of low cloud, where low-altitude (LA) cloud is defined here as cloud topped below 200 m above the surface. Higher-altitude (HA) cloud, or cloud with bases above 200 m, was also sampled during the profiles and transits. The polynyas that were sampled over are shown in the top center of each panel of Fig. 2. Cloud was sampled on eight of the 11 flights, more frequently during period 1 due to safer flight conditions associated with better visual contrast between clouds and surrounding surfaces as well as because period 2 marked the presence of the Canadian Coast Guard Ship Amundsen in Lancaster Sound (bottom center of each panel in Fig. 2) when the flight plans were focused towards sampling of the ship's plume (e.g. Aliabadi et al., 2016c).

All aerosol number concentrations are given in terms of standard atmospheric pressure and temperature (STP: 1 atm and 15^{o}C). The CDNC are also referenced to STP where comparisons are made with the aerosol number concentrations. Number concentrations of particles greater than 100 nm (N100) are taken from the UHSAS. All data, except for the SMS, are 1 second averages that represent a sampling path length of 60–80 m. The size distributions over 20-100 nm are from the SMS data, which are 1-minute averages. Except for the example shown in Fig. S3, all number concentrations of particles between 20 nm and 100 nm are taken from the SMS. Nx-100 refers to the number concentration within the interval “x-100” where x ranges between 20 and 90. Values of Nx with x < 100 are derived from the sum of Nx-100 (SMS) + N100 (UHSAS).

Clouds were sampled when they were present in the area of study, ideally by ascending or descending through them. It was not possible to sample below the base of the LA clouds. Most clouds were liquid phase, and only liquid phase clouds, based on the 2DC-Grey images of cloud particles >50 µm, are discussed here. In addition, none of the liquid clouds exhibited detectable precipitation, with the caveat that droplets in a couple of the lowest altitude clouds were very low in number and relatively large in size (30-40 µm). Considering the settling speeds of such large droplets, they may be considered precipitation. The HA clouds were either stratus or stratocumulus. The LA clouds were fog or stratus. Turbulence was most noticeable in the stratocumulus sampled on July 7, but it was still light. Cloud droplet sizes are represented by the volume-weighted mean diameter (VMD), which has the property that the VMD can be used with CDNC to calculate LWC.

The pre-cloud aerosols for the HA clouds are mostly derived from averages of values collected within about 50 m of cloud base where a cloud base was clear and achievable; in the July 19 case, the estimated pre-cloud aerosol concentrations included a contribution from above cloud. At 200 m or below, the LA clouds were in the boundary layer, indistinguishable from the surface in flight (possibly fog), and sampling below the cloud was not possible due to proximity to the surface. With the exception of the July 8 case, the pre-cloud aerosol for the LA clouds is estimated from aerosol measurements made in the clear air upwind of the cloud. Details of the pre-cloud aerosol estimated for the HA and LA clouds are given in sections 3.2.1 and 2.3.2, respectively. For the aerosol measurements made with the 1-minute averaged number concentrations from the SMS, values from further below-cloud are necessary in some cases. These values are however consistent with the 1-second aerosol measurements closer to cloud base.

A total of 62 liquid water cloud data points were derived from the averages of each cloud penetration with the constraint that the mean LWC is > 0.01 g m^{-3}. The points are integrations over periods ranging from 11 to 1000 seconds with a median sample time of 65 seconds that is equivalent to a horizontal path length of about four kilometers. Some cloud layers were sampled multiple times.

In sections 2.3.1 and 2.3.2, a range of HA and LA examples are used to 1) demonstrate how the pre-cloud aerosol concentrations were assessed for the various points, and 2) note where effects of entrainment may be a factor and how multiple cloud layers are considered. Besides the cloud microphysics, the only in-cloud measurements considered valid inside of cloud are the CO and thermodynamic measurements. For completeness, the aerosol measurements in cloud are included in the figures connected with sections 2.3.1 and 2.3.2, but such measurements, including the CCN, are unreliable due to variability in drying associated with the inlet and a particular instrument as well as droplet shattering on the inlet. The in-cloud aerosol measurements are not used in the subsequent analysis.

2.3.1 Higher Altitude (HA) Cloud Examples

Four examples of profiles through HA clouds are shown in Fig. 3. There are two panels for each profile: the left-hand panel shows CO, CDNC and particle number concentrations (N5, Nx-100, N100, CCNC(0.6%)); the right-hand panel shows temperature, equivalent potential temperature (θ_e), LWC and VMD. The temperatures, θ_e and VMD are scaled as indicated.

July 7 Case (Fig. 3 a, b): This is one of several similar profiles through a stratocumulus layer on July 7 sampled during the transits to and from the polynyas north of Resolute Bay. The CDNC (at STP) are relatively constant with altitude and the LWC and VMD both increase steadily with altitude, features common to the formation of cloud by lifting of air and indicating that the cloud droplets were nucleated on particles in air rising from cloud base. The cloud top is capped by a temperature inversion of about 2^{o}C at 2350 m, and the particle profiles along with θ_e and CO are relatively constant below the cloud base. The only indication from the LWC and CDNC profiles is that entrainment reduces the CDNC. In cloud, the number concentrations of larger particles (N100) is reduced due to nucleation scavenging; although such particles are not completely eliminated as smaller droplets can enter the inlet and dry in the sampling lines. Smaller particles can be artificially increased in cloud due to the shattering of larger droplets on the aerosol intake, as indicated by the increase in the N5 higher in the cloud. The in-cloud aerosol measurements are not used in the subsequent analysis. The CDNC range up to 265 cm^{-3} and the mean value is 199 cm^{-3}. Below cloud base, the N5, N20-100, N30-100, N50-100, N100 and CCNC(0.6%) are approximately 235 cm^{-3}, 167 cm^{-3}, 145 cm^{-3}, 94 cm^{-3}, 67 cm^{-3} and 117 cm^{-3}, respectively. The below-cloud N20 of 234 cm^{-3} approximately equals the N5 providing confidence in the closure of number concentrations. The N30 (N30-100 + N100) compare most closely with the mean CDNC leading to the conclusion that on average cloud droplets nucleated on particles down to about 30 nm. It is possible that particles as small as 20 nm contributed to the CDNC in this cloud based on the maximum CDNC; for 20 nm particles of ammonium sulphate to activate, Köhler equilibrium theory indicates the S in the bases of the clouds would have had to reach above 1.5%.

July 17 Case (Fig. 3 c, d): The maximum and mean CDNC (STP), at about 75 cm^{-3} and 55 cm^{-3}, respectively, are lower and the VMD peak of 20 μm is higher compared with the July 7 profile. The LWC are generally similar between July 7 and July 17, but there are more intervals in the July 17 profile with LWC decreasing from a steady LWC increase associated with an adiabatic lifting. Many of those intervals with decreasing LWC are associated with the aircraft passing through the edges of the stratocumulus during the profile. The inversion topping the cloud is weaker and the peak in the LWC occurs further below cloud top compared with the July 7 case. That LWC feature in combination with the general increase in CO beginning about 660 m suggests that erosion of the cloud top by entrainment was deeper in the July 17 case. Above 660m, the CDNC also decrease; thus the increase in aerosol above cloud did not enhance the CDNC. Continuity from about 100 m below cloud base is indicated by the CO and θ_e profiles, and the N50 approximates the mean CDNC and possibly the maximum CDNC. The CCNC(0.6%) are 30-40 cm^{-3} below cloud, indicating a S larger than 0.6%. The contrast of the July 7 and 17 cases is a relatively simple example of the potential importance of smaller particles for the cloud albedo effect.

July 19 Case (Fig. 3 e, f): The July 19 profile includes two cloud layers, one from 1200-1400 m and the second from 1400-1500 m. The layer separation appears in the CO concentrations that are approximately uniform through the lower layer and increasing in the upper layer. The CO levels of 100+ ppbv in this case are among the highest observed during the study, and transport patterns suggest BB contributed to this aerosol (Köllner et al., Pollution in the summertime Canadian High Arctic observed during NETCARE 2014: Investigation of origin and composition, in Geophysical Research Abstracts, 17, EGU2015-5951, European Geophysical Union General Assembly 2015, Vienna, Austria, 2015). The mean CDNC (STP) in the lower and upper layers are 239 cm^{-3} and 276 cm^{-3} respectively. The VMD reach 15 μm in the lower layer. The VMD are overall smaller and decrease with altitude in the upper layer, consistent with the reduced LWC and increased CDNC. In the upper layer, the CDNC increase from bottom to near the top consistent with the increase in aerosol between below the layer and above the layer. The N50 and N100 estimated for the lower (upper) layer are 269 (334) cm^{-3} and 197 (221) cm^{-3} respectively, where the upper layer values are an average of the aerosol at 1400 m and just above cloud top. On average, the CDNC in both layers are approximated by the activation of particles sized between 50 nm and 100 nm, and comparison with the maximum CDNC suggests activation of particles down to about 50 nm. The CCNC(0.6%) are slightly below the N100, which would be consistent with reduced hygroscopicity of BB particles. Comparison of CCNC(0.6%) and CDNC suggests cloud S above 0.6%.

July 20 Case (Fig. 3 g and h): This is a case of a more complex cloud with variations in the LWC that suggests three cloud layers. The values of the mean CDNC at STP are 45 cm^{-3}, 49 cm^{-3} and 65 cm^{-3} in the upper, middle and lower layers respectively. The VMD reach about 20 μm in the lower layer and 26 μm in the upper layer with the lower CDNC. The layers are relatively stable with CO and θ_e increasing slightly from below the cloud to above the top cloud layer. N50 just below the lower layer approximately equals CDNC in that layer. It is more difficult to estimate the pre-cloud aerosol for the middle and upper layers, but particles at least as small as 50 nm were apparently activated. For the summary statistics, the respective pre-cloud N100, N50 and CCNC(0.6%) are estimated at 24 cm^{-3}, 44 cm^{-3} and 24 cm^{-3} for the upper cloud layer, 32 cm^{-3}, 52 cm^{-3} and 32 cm^{-3} for the middle layer and 34 cm^{-3}, 66 cm^{-3} and 35 cm^{-3} for the lower layer. Comparison of the CCNC(0.6%), which are in approximately the same concentration as the N100, and CDNC suggests S in excess of 0.6%.

2.3.2 Low-Altitude (LA) Examples

July 5 and July 7 Cases: The two examples in Fig. 4 are for cloud or fog over the two polynyas north of Resolute Bay on July 5 and July 7. Four cloud samples were collected on July 5 at altitudes below 200 m. The time series in Fig. 4a covers the period of collection of the two lowest samples: 16:18:02-16:21:57 at 130 m and 16:39:35-16:40:18 at 88 m. In the air upwind of the cloud or fog, the N100, N30 and CCNC(0.6%) are estimated at 3 cm^{-3}, 10-14 cm^{-3} and 5 cm^{-3}. The mean values of the CDNC of 2.8 cm^{-3} at 130 m and 0.7 cm^{-3} at 88 m are explained by N100 and an S that is less than 0.6%. The maximum CDNC of 12 cm^{-3} at 130 m suggests the activation of smaller particles, possibly as small as 30 nm with S exceeding 0.6%, perhaps due to some uplift influenced by orographic features north of the north polynya. At 88 m, the mean VMD (not shown) was 29 µm and ranged up to 35 µm giving those droplets the potential to gravitationally settle over an hour or so, which could result in the transfer of water from the polynya to the downwind ice. On July 7, cloud or fog was present below 120 m and thicker towards the north edge of the north polynya and again to the north over the ice. The CDNC are overall higher with averages of seven samples over the period 16:06-16:29 ranging from 4 cm^{-3} to 13 cm^{-3}. The one-second CDNC are as high as 34 cm^{-3}, and the mean VMD (not shown) range from 19.6 µm to 22.8 µm. The CO mixing ratio is slightly higher within the cloud (81 ppbv) than above (79 ppbv); although this difference may not be significant. In the air nearly free of cloud and below 120 m, the N100 are 4-5 cm^{-3}, the N50 are 8-11 cm^{-3} and the N20 are variable between 17 cm^{-3} and 130 cm^{-3}; CCN are unavailable for this part of the flight due to instrument problems. Mean values of CDNC/N100 and CDNC/N50 for seven cloud samples are 4.8 and 1.0, respectively, indicating that on average particles of about 50 nm were activated in this LA cloud. Based on the overall relationship between CCNC(0.6%) and N50, which is discussed in section 3.3, the mean S in the LA cloud of July 7 is estimated at 0.6%. Comparison with the maximum CDNC suggests that particles as small as 20 nm may have participated in the nucleation of droplets.

July 8 Case: Fig. 5 shows a time series of altitude, CO, N100, N80-100, N90-100, CCNC(0.6%) and CDNC from the sampling above and in the top of low cloud over Lancaster Sound on July 8. The cloud over the open water of the Sound is visible in the satellite picture in Fig. 2b. The general wind direction was from east to west along the Sound. Cloud was also present over the ice to the west, but it was much thinner and reached only to about 150 m above the surface. Over the water, the cloud was sampled as high as 230 m by descending into it to about 150 m as shown in Fig. 5 between 17:27 UT and 17:43 UT. Observations in profiles from two of the five samples are shown in Fig. 6. The cloud deepened as the aircraft approached the ice edge from over the water, and thinned abruptly over the ice with tops below 150 m as shown in Fig. 5 (time 17:47). The thicker cloud was associated with a shift in wind direction to more southerly suggesting an influence of the Prince Regent Inlet and surrounding terrain on the cloud as well as possibly circulations influenced by the water-ice transition. The cloud layer was relatively stable and the θ_e profiles suggest a surface heat sink (Fig. 6a). The profiles of LWC and VMD in Fig. 6 (b, c) do not show increases with altitude characteristic of vertical mixing, such as for some of the HA clouds (Fig. 3); the change in the VMD per 50 m increase in height is about 1.7 µm for the well mixed cloud of July 7 (Fig. 3 a, b) and about 0.2 µm per 50 m for the LA cloud of flight 8 in Fig. 6. The CO mixing ratio shows little variation with time and altitude. The pre-cloud aerosol concentrations are more difficult to assess. Based on concentrations just above the cloud, particles >90 nm explain the CDNC. Based on the concentrations downwind at

150 m (approximately 17:47), activation of particles >80 nm is needed to explain the CDNC. The CCNC(0.6%) are about 129 cm^{-3} downwind and between 157 cm^{-3} and 234 cm^{-3} just above cloud. It is concluded that in this case the droplets likely nucleated on particles mostly larger than 80-95 nm and the S in the clouds were less than 0.6%; although chemical processing in the cloud could have increased the size of the apparent residuals. For the purposes of summary statistics discussed next, the N100, N50 and CCNC(0.6%) have been selected as an average of the downwind and immediately above cloud concentrations: 73 cm^{-3}, 319 cm^{-3} and 168 cm^{-3}, respectively.

3. Summary Observations and Discussion

Summary statistics for the cloud and aerosol samples are discussed in 3.1, the microphysics of the LA and HA clouds are contrasted in 3.2, particle activation is summarized in 3.3 and in section 3.4 the relationship between VMD and CDNC is used to consider the transition of aerosol indirect effects from potential warming to potential cooling. All analyses are based on the 62 cloud points (24 LA points and 38 HA points) as discussed in section 2.3.

3.1 Summary of mean observations

The mean, median, 5th percentile and 95th percentile values of the microphysical properties of the cloud and pre-cloud aerosols as well as the altitudes and temperatures derived from the 62 cloud samples are given in Table 1, separated between periods 1 and 2. Values of the CDNC and the LWC are given relative to in-situ volumes as well as STP. The number of pre-cloud

CCNC(0.6%) samples in Table 1 is limited to 44 due to instrument problems, all of which occurred during the early part of July 7.

Cloud liquid water paths (LWP) were estimated for 33 of the samples when a complete profile between cloud base and cloud top was possible. Summary statistics for the LWP are given at the bottom of Table 1. The 33 LWP estimates are all above 200 m, and respective mean and median altitudes are 1380 m and 1440 m. Of the below-200 m samples, the July 8 case LWP (Figs. 5 and 6) was highest. For the minimum altitude reached in that cloud, the LWP ranged from 12 to 25 indicating that the total LWP exceeded 25.

During period 1, the median sampling altitude is lower and the temperatures are slightly below freezing compared with just above freezing during period 2. The CO mixing ratios are overall low and at approximately background values during period 1. The median CDNC are higher during period 1 than period 2, but the mean values are similar. The CDNC compare more closely with N50 during period 1, while during period 2 the CDNC are between N50 and N100. The CCNC(0.6%) equate with particles between 50 nm and 100 nm for period 1, and for period 2 they are closer to the N100 values. As above, contributions from BB to the aerosol during period 2 may have contributed to the overall reduction in particle hygroscopicity.

3.2 Comparison of LA and HA cloud

The LA clouds were close to the surface and associated with open water; some or all may be fogs. They form by advection of warmer moist air over a cooler surface (the July 8 LA cloud that moved from Baffin Bay westward along Lancaster Sound was likely dominated by that process), by radiation cooling or by the passage of very cold air over a warm moist surface. The latter, also known as sea smoke, is the likely explanation for the observed clouds over the polynyas; it is possible that there was an advection component associated with some of the sea smoke as it moved from the polynyas over the ice surfaces. More generally, the LA clouds are associated with low-level horizontal advection and heat and water exchange with the underlying ice or water surface. In contrast, vertical motions are responsible for many, if not all, of the HA clouds, and none of the HA clouds interacted directly with the underlying surface. Due to the differences in formation processes, the characteristics of the LA and HA clouds are considered separately. Table 2 shows the mean, median, 5th percentile and 95th percentile values for the samples separated between LA and HA clouds; the vertical distributions of CDNC, LWC and VMD samples are shown in Supplement Fig. S6. On average, the LA samples have lower CDNC and higher VMD compared with the HA cases, and the LA clouds are activating on larger particles relative to the HA clouds as indicated by CDNC/N50. The values of the CDNC/CCNC(0.6%) indicate that the average S are <0.6% for the LA clouds and close to 0.6% for the HA clouds.

Variations in LWC are correlated with those of CDNC for the LA samples (Fig. 7a). The coefficient of determination (R^2) rises from 0.57 to 0.98 if the one LA point at (137, 0.032) is removed. In contrast, the correlation of the LWC with the CDNC for the HA samples is low (R^2=0.12). There is no correlation of the LWC with the VMD for the LA points (R^2=0.04), and for the HA clouds there is a modest correlation of LWC with MVD (R^2=0.26). Variations in LWC with VMD within a cloud system are consistent with lifting of air from below, i.e. nucleation of droplets at cloud base followed by their growth with increasing altitude, such as the case shown in Fig. 3a and 3b. Variations of LWC with VMD can also result from homogeneous mixing (i.e. entrainment of dry air that reduces LWC by partial evaporation of droplets without reducing CDNC). The strong dependence of the variations in LWC with those of the CDNC in the LA clouds may reflect changes in rate of cooling, collision-coalescence or inhomogeneous mixing along the cloud transport pathway. For example, increases in the rate of cooling within or between clouds will increase condensation rates, and potentially S, resulting in increased LWC and CDNC. Changes in collision-coalescence will affect the CDNC and LWC in similar ways: more collision-coalescence, lower CDNC and lower LWC due to precipitation. Inhomogeneous mixing, the entrainment of dry air parcels into a cloud without mixing with the cloud droplets, will reduce the CDNC averaged across the cloud and at the same time reduce the mean LWC. Changes in the aerosol that are interactive with some of the cloud processes may contribute to the CDNC and potentially the LWC through their influence on collision-coalescence. The LWC-CDNC correlations are identifiable not just for the combined LA points, but also for individual LA clouds (see Supplement Fig. S7). Greater temporal and spatial coverage are needed to assess the microphysical processes in these clouds.

3.3 Particle Activation Sizes

Here, the sizes and CCN activity of particles that acted as nuclei for cloud droplets are examined. The CDNC are plotted versus N100 in Fig. 8a, separated between LA and HA samples. The CDNC are most often higher than the N100 and more so for the HA samples, which indicates that particles smaller than 100 nm activated in most cases and most often in the HA clouds. The mean and median values of CDNC(STP)/N100 are 2.2 and 1.8 for all 62 samples, and the 30th percentile of the CDNC/N100 is 1.2, which means that in about 70 % of the cases droplets nucleated on particles significantly smaller than 100 nm. Fig. 8a can be compared with the results of Hegg et al. (2012) who showed a linear fit of CDNC to N100 for marine stratocumulus with a slope of 0.72 for which the N100 in 94% of the samples was >150 cm^{-3}. Here, a slope larger than unity is indicated, and the N100 are <100 cm^{-3} in 90% of the samples. The comparison indicates that relationships derived for higher concentration environments do not necessarily apply to those of lower concentration environments. In the clean environment often found in the Arctic during summer, the absence of larger particles may lower water uptake rates during droplet nucleation, which will increase the S, enabling cloud droplets to nucleate on smaller particles; the absence of larger particles may also help increase the concentrations of smaller particles in the Arctic during summer, by promoting new particle formation through a reduced condensation sink (e.g. Strom et al., 2003; Engvall et al., 2008). The CDNC are plotted against the N50 in Fig. 8b showing that the mean activation size of the HA clouds was often close to 50 nm. The median value of CDNC/N50 is 0.78 for all samples indicating that, based on the averaged CDNC, cloud droplets nucleated on particles near or smaller than 50 nm about 40% of the time. That percentage will increase if particle activation is considered relative to the maximum CDNC associated with any cloud sample.

The mean and median values of the CCNC(0.6%) associated with all cloud samples (84 cm^{-3} and 47 cm^{-3}) are generally consistent with previous Arctic CCNC measurements. For example, during the summer above 85°N, Martin et al. (2011) measured a mean CCNC at 0.73% S of 47 cm^{-3} with a standard deviation of 35 cm^{-3}, Yum and Hudson (2001) measured CCNC at 0.8% S below 1700 m over the Beaufort Sea during May, 1998 that ranged from 41 cm^{-3} to 290 cm^{-3}, and Radke et al. (1976) measured a mean CCNC at 1% S of 90 cm^{-3} in June near Barrow, Alaska. Considering the median values of CDNC/CCNC(0.6%) for the LA and HA samples (Table 2) and the slopes of linear regressions of CDNC versus CCNC(0.6%) (Fig. 9a), the average S inferred for these HA clouds is about 0.6%, consistent with the overall activation of smaller particles in those clouds. The mean S inferred for the LA clouds is significantly lower than 0.6%. Based on the activation of a 90 nm particle (July 8 case; CCNC(0.6%) of 168 cm^{-3} in Fig. 10a) of low-moderate hygroscopicity, a reasonable estimate is 0.3% for the mean of the LA clouds with some higher values indicated by the points near a CCNC(0.6%) of 25 cm^{-3} in Fig. 9a. The S for these clean clouds are in contrast to polluted marine environments for which estimates for these types of clouds are 0.2% or less (e.g. Modini et al., 2015). Consistent with the present results, Hudson et al. (2010) found that effective S in marine stratus tended to increase with a decrease in the CCNC, and for CCNC lower than about 200 cm^{-3} the effective S ranged between 0.3% and 1.2%.

Variations in the measured CCNC(0.6%) are explained well by variations in smaller (N50) and larger (N100) particles as shown in Fig. 9b. The slopes of the power-law fits, for which the exponents are both close to unity, indicate that the CCNC(0.6%) on average fall between 50 nm and 100nm.

3.4 Aerosol Influences on Warming to Cooling

The relationship between the VMD and CDNC shown in Fig. 10 exhibits a scattered but clear tendency for smaller VMD with increasing CDNC. The solid black curve is a reference line based on the study-mean LWC of 0.12 g m^{-3} (Table 1); points falling above or below the black curve have higher or lower LWC, respectively. The vertical dashed green line represents our best estimate of the Mauritsen limit below which Mauritsen et al. (2011) showed that cloud may produce a net warming for an increase in the CDNC. The net warming is a consequence of an increase in longwave absorption due to an increase in the LWC, where the latter results from a reduction in deposition for the smaller droplets associated with increased CDNC. A value of 16 cm^{-3} is our best estimate of the Mauritsen limit for this data set because all points with CDNC below that value fall well below the mean LWC, therefore offering greater potential for changes in the CDNC to increase the LWC. Above the estimated Mauritsen limit, an increase in CDNC may produce a net cooling due to the cloud albedo effect, since at that point the longwave forcing does not change significantly as the effects of deposition are reduced and the cloud effectively behaves as a black body; the LA cloud of July 8 is an example.

The aerosol influence on clouds with CDNC below the Mauritsen-limit is considered in section 3.4.1. In section 3.4.2, the potential background influence of the aerosol on clouds with CDNC above the Mauritsen-limit is discussed.

3.4.1 Below the Mauritsen limit

Seventeen of the 62 samples fall at or below our best estimate of the Mauritsen limit. Fifteen of those 17 samples are from LA clouds with median pre-cloud N50 and N100 estimates of 8.2 cm^{-3} and 3.0 cm^{-3} respectively. The lower number concentrations contribute to overall larger VMD. Increases in small particles, potentially from particle nucleation or fragmentation (e.g. Leck and Bigg, 1999 and 2010), are hypothesized to increase the CDNC thereby enhancing longwave warming by these clouds, at least until the CDNC reach above the estimated Mauritsen limit. The LA points from the July 5 and the July 7 cases, identified in Fig. 10, offer one insight. The median CDNC for July 5 is six times lower than the July 7 CDNC: 1.3 cm^{-3} and 7.8 cm^{-3}, for July 5 and 7, respectively. The median N50 are 6 cm^{-3} and 8.3 cm^{-3} for July 5 and 7, respectively, and the median N100 are 3 cm^{-3} and 2.2 cm^{-3} for July 5 and July 7, respectively. The CDNC are similar to N50 in the July 7 case, but lower than both the N50 and N100 in the July 5 case indicating the aerosol was not a limiting factor in the July 5 case. Consistent with the discussion in section 3.2, all 15 LA points below the Mauritsen limit show a correlation of LWC with the CDNC (R^2=0.57), but correlations of CDNC with N50 and N100 are weak at best: R^2=0.19 and 0.06, respectively. The CCN are not used here because only seven points with CCNC(0.6%) are available; those seven points do correlate with the N50. If the limit of 10 cm^{-3} of Mauritsen et al. (2011) is applied, reducing the number of points to 12, the assessment does not change: the LWC-CDNC correlation improves slightly and the correlations of the CDNC with the N100 and the N50 weaken. The LWC do not correlate with either the N50 or the N100 (Supplement Fig. S8), suggesting that small changes in the aerosol alone within the Mauritsen limit do not have a profound effect on the LWC. Larger changes in the aerosol may shift the LA cloud into the region above the Mauritsen limit, which appears to be the case for July 8.

3.4.2 Background aerosol influence on clouds

Above the estimated Mauritsen limit, the general reduction in the VMD with the CCNC(0.6%)-associated increase in CDNC reflects the impact of increases in aerosol on clouds. In Fig. 10, samples are identified between those associated with lower CO (green circles; <81 ppbv, the median CO value of all samples) and those with highest CO (red circles; >90 ppbv); six samples have no CO measurement and the remaining points have CO falling within 81-90 ppbv. Five of the seven higher-CO samples are from the July 19 case (e.g. Fig. 3e, 3f) that has been linked with BB (Köllner et al., 2015; reference above), and the highest CDNC point (273 cm^{-3}; no CO measurement) is also from July 19 and likely influenced by BB. The higher CO samples cover a range of CDNC from 16 cm^{-3} to at least 238 cm^{-3} with CO reaching up to 113 ppbv. Consistent with a BB influence, the higher CO points are associated with nearly three times as many larger particles (N100=149 cm^{-3}) compared with the lower CO samples (N100=58 cm^{-3}). The higher CO points fall at the low end of the observations from Zamora et al. (2015), but their CO concentrations are much higher than those measured in this study. The lower-CO samples may be dominated by regional biogenic emissions (Willis et al., 2016). The lower- and higher-CO points overlap over a CDNC range of 16 cm^{-3} to 160 cm^{-3}, consistent with the range of pre-industrial CDNC from global models of 30 cm^{-3} to 140 cm^{-3} (Penner et al., 2006). In this clean environment, the contributions from 20-100 nm particles have a broad impact on the range of CDNC, affirming the large uncertainty associated with estimating a baseline for the cloud albedo effect discussed by Carslaw et al. (2013).

4. Summary and Conclusions

Aerosol particle size distributions, CCNC at 0.6% water supersaturation or CCNC(0.6%), carbon monoxide (CO) and cloud microphysics were measured from an airborne platform based out of Resolute Bay, Nunavut from July 4 to July, 21, 2014 as one part of the Canadian NETCARE project. The flights were conducted over ice and water surfaces from about 60 m above the surface to about 6000 m. Sixty-two (62) cloud-averaged points were derived, each constrained for the mean LWC >0.01 g m^{-3}: the cloud threshold used here. The analysis separates the cloud samples between 24 low-altitude (LA: tops below 200 m) samples and 38 higher altitude (HA: bases above 200 m) samples as well as situations of lower and higher CO and observations above and below the Mauritsen et al., (2011) CCN limit.

The overall median pre-cloud N100 of 33 cm^{-3} and the median CO mixing ratio of 81 ppbv indicate that the aerosols supporting the sampled clouds were relatively clean, and particularly during the first part of the study many of the aerosol particles may have been derived from regional natural sources (Willis et al., 2016). The median CDNC at STP is 10 cm^{-3} for the LA clouds and 101 cm^{-3} for the HA clouds, which correspond with the median pre-cloud N50 of 11 cm^{-3} for the LA samples and 133 cm^{-3} for the HA samples. The lower sizes of particles activated in cloud varied from about 20 nm to above 100 nm. In 40% of cases, the average lower size of activation was 50 nm or smaller. Overall, smaller particles were activated more often in the HA clouds. Variations in particle chemistry will induce some variance in these results, but because activation diameters are estimated starting with larger particles and moving to smaller sizes, changes in chemistry only offer the possibility of activation of particles still smaller than estimated here.

From the median values of CDNC/CCNC(0.6%) (1.2 for the HA clouds and 0.6 for the LA clouds) and the linear regression of CDNC and CCNC(0.6%), it is inferred that the average S were approximately 0.6% for the HA clouds and 0.3% for the LA clouds. Higher estimates will be obtained if the maximum CDNC are taken into consideration rather than the mean CDNC. The relatively high S for these clean Arctic stratus and stratocumulus have similarities with the observations of Hudson et al. (2010) for relatively clean stratus off the coast of California.

In 17 cases, 15 of which were LA clouds, the CDNC fell at or below the CCN limit discussed by Mauritsen et al. (2011), which is estimated here as 16 cm^{-3}. These are the first collection of simultaneous observations of the microphysics of aerosols and clouds in this unique regime in which the net radiative impact of increases in the CDNC is hypothesized to be warming due to changes in the LWC. The LWC of the points below the Mauritsen limit all fall below the study-mean LWC, and the LWC increases with the CDNC. Neither the CDNC nor the LWC are positively correlated with the pre-cloud aerosol (N50 or N100). In this environment of low cloud or fog and ultra-low CDNC, variations in cloud processes such as mixing or the rate of cooling may be responsible for the association of CDNC and LWC.

Forty-five cloud samples with CDNC above the Mauritsen limit exhibit a clear influence of changing aerosol. The cloud microphysics for the clouds formed in cleaner air (smaller particles and lower CO: <81 ppbv) overlap with the microphysics of clouds formed in seemingly more polluted air (larger particles and higher CO: >90 ppbv) covering a CDNC range of 16-160 cm^{-3}. It is concluded that 20-100 nm particles from natural sources can have a broad impact on the range of CDNC in clean environments, such as the summertime Arctic, affirming a large uncertainty in estimating a baseline for the cloud albedo effect.

Acknowledgements. The complete data set is available from the NETCARE web site by contacting Richard Leaitch (Richard.Leaitch@ec.gc.ca) or Jon Abbatt (jabbatt@chem.utoronto.ca). A spreadsheet containing the details of the 62 samples discussed here is included with the supplement. The authors acknowledge a large number of people for their contributions to this work. We thank Kenn Borek Air, in particular Kevin Elke and John Bayes for their skillful piloting that facilitated these cloud observations. We are grateful to John Ford, David Heath and the U of Toronto machine shop, Jim Hodgson and Lake Central Air Services in Muskoka, Jim Watson (Scale Modelbuilders, Inc.), Julia Binder and Martin Gerhmann (AWI), Mike Harwood and Andrew Elford (EC), for their support of the integration of the instrumentation and aircraft. We thank Mohammed Wasey for his support of the instrumentation during the integration and in the field. We are grateful to Carrie Taylor (EC), Bob Christensen (U of T), Kevin Riehl (Kenn Borek Air), Lukas Kandora, Manuel Sellmann and Jens Herrmann (AWI), Desiree Toom, Sangeeta Sharma, Dan Veber, Andrew Platt, Anne Marie Macdonald, Ralf Staebler and Maurice Watt (EC), Kathy Law and Jennie Thomas (LATMOS) for their support of the study. We thank the Biogeochemistry department of MPIC for providing the CO instrument and Dieter Scharffe for his support during the preparation phase of the campaign. We thank the Nunavut Research Institute and the Nunavut Impact Review Board for licensing the study. Logistical support in Resolute Bay was provided by the Polar Continental Shelf Project (PCSP) of Natural Resources Canada under PCSP Field Project #218-14, and we are particularly grateful to Tim McCagherty and Jodi MacGregor of the PCSP. Funding for this work was provided by the Natural Sciences and Engineering Research Council of Canada through the NETCARE project of the Climate Change and Atmospheric Research Program, the Alfred Wegener Institute and Environment Canada.

References

Aliabadi, A. A., R. M. Staebler, J. de Grandpré, A. Zadra, P. A. Vaillancourt: Comparison of Estimated Atmospheric Boundary Layer Mixing Height in the Arctic and Southern Great Plains under Statically Stable Conditions: Experimental and Numerical Aspects, Atmosphere-Ocean, 54, 60-74, doi: 10.1080/07055900.2015.1119100, 2016a.

Aliabadi, A. A., R. M. Staebler, M. Liu, and A. Herber: Characterization and Parametrization of Reynolds Stress and Turbulent Heat Flux in the Stably-Stratified Lower Arctic Troposphere Using Aircraft Measurements, Boundary-Layer. Meteorol., In Press, doi: 10.1007/s10546-016-0164-7, 2016b.

Aliabadi, A.A., J. L. Thomas, A. Herber, R. M. Staebler, W. R. Leaitch, K. S. Law, L. Marelle, J. Burkart, M. Willis, J. P. D. Abbatt, H. Bozem, P. Hoor, F. Köllner, J. Schneider, and M. Levasseur. Ship emissions measurement in the Arctic from plume intercepts of the Canadian Coast Guard Amundsen icebreaker from the Polar 6 aircraft platform. Atmos. Chem. Phys. Discuss., doi: 10.5194/acp-2015-1032, 2016c.

Barrie, L.A.: Arctic air pollution: An overview of current knowledge, Atmos. Environ., 20, 643–663, doi:10.1016/0004-6981(86)90180-0, 1986.

Barrie, L.A., Bottenheim, J.W., Schnell, R.C., Crutzen, P.J., and Rasmussen, R.A.: Ozone depletion and photochemical reactions at polar sunrise in the lower Arctic atmosphere, Nature, 334, 138-141, 1998.

Brenner, T.C., Curry, J.A., and Pinto, J.O.: Radiative transfer in the summertime Arctic, J. Geophys. Res., 106, 15173-15183, 2001.

Brock, C.A., Cozic, J., Bahreini, R., Froyd, K.D., Middlebrook, A.M., McComiskey, A., Brioude, J., Cooper, O.R., Stohl, A., Aikin, K.C., de Gouw, J.A., Fahey, D.W., Ferrare, R.A., Gao, R.-S., Gore, W., Holloway, J.S., Hubler, G., Jefferson, A., Lack, D.A., Lance, S., Moore, R.H., Murphy, D.M., Nenes, A., Novelli, P.C., Nowak, J.B., Ogren, J.A., Peischl, J., Pierce, R.B., Pilewskie, P., Quinn, P.K., Ryerson, T.B., Schmidt, K.S., Schwarz, J.P., Sodemann, H., Spackman, J.R., Stark, H., Thomson, D.S., Thornberry, T., Veres, P., Watts, L.A., Warneke, C., and Wollny, A.G.: Characteristics, sources, and transport of aerosols measured in spring 2008 during the aerosol, radiation, and cloud processes affecting Arctic climate (ARCPAC) project, Atmos. Chem. Phys., 11, 2423–2453, 2011, doi:10.5194/acp-11-2423-2011, 2011.

Browse, J., Carslaw, K.S., Mann, G.W., Birch, C.E., Arnold, S.R., and Leck, C.: The complex response of Arctic aerosol to sea-ice retreat, Atmos. Chem. Phys., 14, 7543-7557, doi:10.5194/acp-14-7543-2014, 2014.

Burkart, J., Willis, M., Köllner, F., Schneider, J., Bozem, H., Hoor, P., Ghahremaninezhadgharelar, R., Wentworth, G., Norman, A.L., Brauner, R., Konrad, C., Herber, A., Leaitch, R., and Abbatt, J.P.D.: Evidence for New Particle Formation in the Summertime

Arctic near Resolute Bay, Nunavut, Canada, presented at the 7th Symposium on Aerosol–Cloud–Climate Interactions, American Meteorological Society, Phoenix, Arizona, 2015.

Cai, Y., Montague, D.C., Mooiweer-Bryan, W., Deshler, T.: Performance characteristics of the ultra-high sensitivity aerosol spectrometer for particles between 55 and 800 nm: Laboratory and field studies, J. Aerosol Sci., 39, 759 – 769, 2008.

Carslaw, K.S., Lee, L.A., Reddington, C.L., Pringle, K.J., Rap, A., Forster, P.M., Mann, G.W., Spracklen, D.V., Woodhouse, M.T., Regayre, L.A., and Pierce, J.R.: Large contribution of natural aerosols to uncertainty in indirect forcing. Nature, 503, doi:10.1038/nature12674, 2013.

Christensen, J. H. et al.: Chapter 14, in Climate Change 2013, The Physical Science Basis (editors Stocker, T. F. et al.), Intergovermental Panel on Climate Change, Cambridge Univ. Press, Cambridge, U.K, 2013.

Curry, J.A.: Introduction to special section: FIRE Arctic clouds experiment, J. Geophys. Res., 106, 14,985-14,987, 2001.

Earle, M. E., Liu, P.S.K., Strapp, J.W., Zelenyuk, A., Imre, D., McFarquhar, D.M., Shantz, N.C., and Leaitch, W.R.: Factors influencing the microphysics and radiative properties of liquid-dominated Arctic clouds: Insight from observations of aerosol and clouds during ISDAC (2008), J. Geophys. Res., 116, D00T09, doi:10.1029/2011JD015887, 2011.

Engvall, A-C, Krejci, R., Strom, J., Treffeisen, R., Scheele, R.: Changes in aerosol properties during spring-summer period in the Arctic troposphere, Atmos. Chem. Phys., 8, 445–462, doi:10.5194/acp-8-445-2008, 2008.

Garrett, T. J., Zhao, C., Dong, X., Mace, G.G., Hobbs, P.V.: Effects of varying aerosol regimes on low-level Arctic stratus, Geophys. Res. Lett., 31, L17105, doi:10.1029/2004GL019928, 2004.

Garrett, T. J., Maestas, M.M., Krueger, S.K., and Schmidt C.T.: Acceleration by aerosol of a radiative-thermodynamic cloud feedback influencing Arctic surface warming, Geophys. Res. Lett., 36, L19804, doi:10.1029/2009GL040195, 2009.

Heintzenberg, J., and Leck C.: Seasonal-variation of the atmospheric aerosol near the top of the marine boundary layer over Spitsbergen related to the Arctic sulphur cycle, Tellus B, 46, 52–67, doi.: 10.1034/j.1600-0889.1994.00005.x, 1994.

Heintzenberg, J., Leck, C., Birmili, W.,Wehner, B., Tjernström, M., and Wiedensohler, A.: Aerosol number-size distributions during clear and fog periods in the summer high Arctic: 1991, 1996, and 2001, Tellus, 58B, 41–50, 2006.

Heintzenberg, J., Leck, C., and Tunved, P.: Potential source regions and processes of aerosol in the summer Arctic, Atmos. Chem. Phys., 15, 6487–6502, doi:10.5194/acp-15-6487-2015, 2015.

Hegg, D.A., Covert, D.S. Jonsson, H.H., and Woods, R.K.: A simple relationship between cloud drop number concentration and precursor aerosol concentration for the regions of earth's large marine stratocumulus decks, Atmos. Chem. Phys., 12, 1229–1238, doi:10.5194/acp-12-1229-2012, 2012.

Herman, G.F.: Solar radiation in summertime Arctic stratus clouds. J. Atmos. Sci., 34, 1423-1432, 1977.

Hobbs, P.V. and Rango, A.L.: Microstructures of low and middle-level clouds over the Beaufort Sea, Q. J. R. Meteorol. Soc., 124, 2035-2071, 1998.

Hudson, J.G., Noble, S., and Jha, V.: Stratus cloud S, Geophys. Res. Lett., 37, L21813, doi:10.1029/2010GL045197, 2010.

Intrieri, J. M., Shupe, M.D., Uttal, T., and McCarty, B.J.: An annual cycle of Arctic cloud characteristics observed by radar and lidar at SHEBA, J. Geophys. Res., 107, C10, 8030, doi. 10.1029/2000JC000423, 2002.

Jacob, D.J., Crawford, J. H., Maring, H., Clarke, A.D., Dibb, J.E., Emmons, L.K., Ferrare, R.A., Hostetler, C.A., Russell, P.B., Singh, H.B., Thompson, A.M., Shaw, G.E., McCauley, E., Pederson, J.R., and Fisher J.A.: The Arctic research of the composition of the troposphere from aircraft and satellites (ARCTAS) mission: Design, execution, and first results, Atmos. Chem. Phys., 10, 5191–5212, doi:10.5194/acp-10-5191-2010, 2010.

Jouan, C., Pelon, J., Girard, E., Ancellet, G., Blanchet, J.P., and Delanoë, J.: On the relationship between Arctic ice clouds and polluted air masses over the North Slope of Alaska in April 2008, Atmos. Chem. Phys., 14, 1205–1224, doi:10.5194/acp-14-1205-2014, 2014.

Klingebiel, M., de Lozar, A., Molleker, S., Weigel, R., Roth, A., Schmidt, L., Meyer, J., Ehrlich, A., Neuber, R., Wendisch, M., and Borrmann, S.: Arctic low-level boundary layer clouds: In situ measurements and simulations of mono- and bimodal supercooled droplet size distributions at the top layer of liquid phase clouds, Atmos. Chem. Phys., 15, 617–631, doi:10.5194/acp-15-617-2015, 2015.

Korhonen, H., K. S. Carslaw, D. V. Spracklen, D. A. Ridley, and J. Ström: A global model study of processes controlling aerosol size distributions in the Arctic spring and summer, J. Geophys. Res., 113, D08211, doi:10.1029/2007JD009114, 2008.

Korolev, A.V., Emery, E.F., Strapp, J.W., Cober, S.G., Isaac, G.A., Wasey, M., and Marcotte, D.: Small ice particles in tropospheric clouds: fact or artifact? Airborne icing instrumentation evaluation experiment, B. Am. Meteorol. Soc., 92, 967–973, 2011.

Lance, S., Shupe, M.D., Feingold, G., Brock, C.A., Cozic, J., Holloway, J.S., Moore, R.H., Nenes, A., Schwarz, J.P., Spackman, J.R., Froyd, K.D., Murphy, D.M., Brioude, J., Cooper, O.R., Stohl, A., and Burkhart J.F.: Cloud condensation nuclei as a modulator of ice processes in

Arctic mixed-phase clouds, Atmos. Chem. Phys., 11, 8003–8015, doi:10.5194/acp-11-8003-2011, 2011.

Law, K.S., and Stohl, A.: Arctic air pollution: origins and impacts, Science, 315, 1537–1540, 2007.

Leaitch W. R., Lohmann, U., Russell, L.M., Garrett, T., Shantz, N.C., Toom-Sauntry, D., Strapp, J.W., Hayden, K.L., Marshall, J., Wolde, M., Worsnop, D.R., Jayne, J.T.: Cloud albedo increase from carbonaceous aerosol, Atmos. Chem. Phys., 10, 7669-7684, doi:10.5194/acp-10-7669-2010, 2010.

Leaitch, W.R., Sharma, S., Huang, L., Macdonald, A.M., Toom-Sauntry, D., Chivulescu, A., von Salzen, K., Pierce, J.R., Shantz, N.C., Bertram, A., Schroder, J., Norman, A.-L., and Chang R.Y.-W.: Dimethyl sulphide control of the clean summertime Arctic aerosol and cloud, Elementa: Science of the Anthropocene, 1, 000017, doi: 10.12952/journal.elementa.000017, 2013.

Leck C., and Bigg, E.K.: Aerosol production over remote marine areas - A new route, Geophys. Res. Lett., 26, 3577-3580, 1999.

Leck C., and Bigg, E. K.: New particle formation of marine biological origin, Aerosol Sci. Technol., 44, 570–577, doi:10.1080/02786826.2010.481222, 2010.

Lohmann, U., Humble, J., Leaitch, R., Isaac, G., and Gultepe, I.: Simulations of ice clouds during FIRE.ACE using the CCCMA single column model, J. Geophys. Res., 106, 15123-15138, 2001.

Lohmann, U. and Leck, C.: Importance of submicron surface active organic aerosols for pristine Arctic clouds, Tellus B, 57, 261–268, 2005.

Lubin, D. and Vogelmann, A.M.: Observational quantification of a total aerosol indirect effect in the Arctic, Tellus, 62B, 181–189, DOI: 10.1111/j.1600-0889.2010.00460.x, 2010.

Martin, M., Chang, R.Y.-W., Sierau, B., Sjogren, S., Swietlicki, E., Abbatt, J.P.D., Leck, C., and Lohmann, U.: Cloud condensation nuclei closure study on summer arctic aerosol, Atmos. Chem. Phys., 11, 11335–11350, doi:10.5194/acp-11-11335-2011, 2011.

Maslanik, J., Stroeve, J., Fowler, C., and Emery, W.: Distribution and trends in Arctic sea ice age through spring 2011, Geophys. Res. Lett., 38, L13502, doi:10.1029/2011gl047735, 2011, 2011.

Mauritsen, T., Sedlar, J., Tjernström, M., Leck, C., Martin, M., Shupe, M., Sjogren, S., Sierau, B., Persson, P.O.G., Brooks, I.M., and Swietlicki E.: An Arctic CCN-limited cloud-aerosol regime, Atmos. Chem. Phys., 11, 165–173, doi:10.5194/acp-11-165-2011, 2011.

Modini, R.L., Frossard, A.A., Ahlm, L., Russell, L.M., Corrigan, C.E., Roberts, G.C., Hawkins, L.N., Schroder, J.C., Bertram, A.K. Zhao, R., Lee, A.K.Y., Abbatt, J.P.D., Lin, J., Nenes, A., Wang, Z., Wonaschütz, A., Sorooshian, A., Noone, K.J., Jonsson, H., Seinfeld, J.H., Toom-Sauntry, D., Macdonald, A.M., and Leaitch W.R.: Primary marine aerosol-cloud interactions off the coast of California, J. Geophys. Res. Atmos., 120, 4282–4303, doi:10.1002/2014JD022963, 2015.

Morrison, H., de Boer, G., Feingold, G., Harrington, J., Shupe, M.D., and Sulia K.: Resilience of persistent Arctic mixed-phase clouds, Nat. Geosci., 5, 11–17, doi:10.1038/ngeo1332, 2012.

Najafi, M. R., Zwiers, F.W. and Gillett N.P.: Attribution of Arctic temperature change to greenhouse-gas and aerosol influences. Nature Climate Change, doi: 10.1038/NCLIMATE2524, 2015.

Peng, Y., Lohmann, U., and Leaitch, R.: The cloud optical depth – cloud droplet effective radius relationship for clean and polluted clouds from RACE and FIRE.ACE. J. Geophys. Res., 107, 4106, 10.1029/2000JD000281, 2002.

Penner J.E., Quaas, J., Storelvmo, T., Takemura, T., Boucher, O., Guo, H., Kirkevåg, A., Kristjánsson, J.E., and Seland, Ø.: Model intercomparison of indirect aerosol effects, Atmos. Chem. Phys., 6, 3391–3405. doi:10.5194/acp-6-3391-2006, 2006.

Quinn, P.K., Bates, T.S., Baum, E., Doubleday, N., Fiore, A.M., Flanner, M., Fridlind, A., Garrett, T.J., Koch, D., Menon, S., Shindell, D., Stohl, A., and Warren S.G.: Short-lived pollutants in the Arctic: Their climate impact and possible mitigation strategies, Atmos. Chem. Phys., 8, 1723–1735, doi:10.5194/acp-8-1723-2008, 2008.

Radke, L.F., P.V. Hobbs, and Pinnons, J.E.: Observations of cloud condensation nuclei, sodium-containing particles, ice nuclei and the light-scattering coefficient near Barrow, Alaska, J. Appl. Meteor., 15, 982-995, 1976.

Sandvik, A., Biryulina, M., Kvamsto, N., Stamnes, J., and Stamnes, K.: Observed and simulated microphysical composition of Arctic clouds: Data properties and model validation, J. Geophys. Res., 112, D05205, doi:10.1029/2006JD007351, 2007.

Shindell, D.T., Chin, M., Dentener, F., Doherty, R.M., Faluvegi, G., Fiore, A.M., Hess, P., Koch, D.M., MacKenzie, I.A., Sanderson, M.G., Schultz, M.G., Schulz, M., Stevenson, D.S., Teich, H., Textor, C., Wild, O., Bergmann, D.J., Bey, I., Bian, H., Cuvelier, C., Duncan, B.N., Folberth, G., Horowitz, L.W., Jonson, J., Kaminski, J.W., Marmer, E., Park, R., Pringle, K.J., Schroeder, S., Szopa, S., Takemura, T., Zeng, G., Keating, T.J., and Zuber, A.: A multi-model assessment of pollution transport to the Arctic, Atmos. Chem. Phys., 8, 5353–5372, doi:10.5194/acp-8-5353-2008, 2008.

Shupe, M.D., Kollias, P., Matrosov, S.Y., and Schneider, T.L.: Deriving mixed-phase cloud properties from Doppler radar spectra, J. Atmos. Ocean. Technol., 21, 660-670, 2004.

Shupe, M.D., Persson, P.O.G., Brooks, I.M., Tjernström, M., Sedlar, J., Mauritsen, T., Sjogren, S., and Leck, C.: Cloud and boundary layer interactions over the Arctic sea ice in late summer, Atmos. Chem. Phys., 13, 9379–9400, doi:10.5194/acp-13-9379-2013, 2013.

Stohl A.: Characteristics of atmospheric transport into the Arctic troposphere, J. Geophys. Res., 111, D11306, doi:10.1029/2005JD006888, 2006.

Stohl, A., Klimont, Z., Eckhardt, S., Kupiainen, K., Shevchenko, V.P., Kopeikin, V.M., and Novigatsky, A.N.: Black carbon in the Arctic: the underestimated role of gas flaring and residential combustion emissions, Atmos. Chem. Phys., 13, 8833–8855, doi:10.5194/acp-13-8833-2013, 2013.

Ström, J., Umegård, J., Tørseth, K., Tunved, P., Hansson, H.-C., Holmém, K., Wismann, V., Herber, A., König-Langlo, G.: One year of particle size distribution and aerosol chemical composition measurements at the Zeppelin Station, Svalbard, March 2000–March 2001, Physics and Chemistry of the Earth 28 (2003) 1181–1190, 2003.

Tjernström, M., Leck, C., Persson, P.O.G., Jensen, M.L., Oncley, S.P., and Targino, A.: The summertime Arctic atmosphere: Meteorological measurements during the Arctic Ocean experiment 2001 (AOE-2001), B. Am. Meteor. Soc., 85, 1305–1321, 2004, 2004.

Tjernström, M., Leck, C., Birch, C.E., Bottenheim, J.W., Brooks, B.J., Brooks, I.M., Bäcklin, L., Chang, R.Y.-W., de Leeuw, G., Di Liberto, L., de la Rosa, S., Granath, E., Graus, M., Hansel, A., Heintzenberg, J., Held, A., Hind, A., Johnston, P., Knulst, J., Martin, M., Matrai, P.A., Mauritsen, T., Müller, M., Norris, S.J., Orellana, M.V., Orsini, D.A., Paatero, J., Persson, P.O.G., Q. Gao, Rauschenberg, C., Ristovski, Z., Sedlar, J., Shupe, M.D., Sierau, B., Sirevaag, A., Sjogren, S., Stetzer, O., Swietlicki, E., Szczodrak, M., Vaattovaara, P., Wahlberg, N., Westberg, M., and Wheeler, C.R.: The Arctic summer cloud ocean study (ASCOS): Overview and experimental design, Atmos. Chem. Phys., 14, 2823–2869, doi:10.5194/acp-14-2823-2014, 2014.

Tunved, P., Ström, J., Krejci R.: Arctic aerosol life cycle: linking aerosol size distributions observed between 2000 and 2010 with air mass transport and precipitation at Zeppelin station, Ny-Alesund, Svalbard, Atmos. Chem. Phys., 13, 3643-3660, doi:10.5194/acp-13-3643-2013, 2013.

United Nations Environment Programme, Near-term Climate Protection and Clean Air Benefits: Actions for Controlling Short-Lived Climate Forcers, UNEP, Nairobi, Kenya, http://www.unep.org/publications/ebooks/SLCF/, 2011.

Yum, S.S., and Hudson, J.G.: Vertical distributions of cloud condensation nuclei spectra over the springtime Arctic Ocean, J. Geophys. Res., 106, 15045–15052, doi:10.1029/2000JD900357, 2001.

Zamora, L.M., Kahn, R.A., Cubison, M.J., Diskin, G.S., Jimenez, J.L., Kondo, Y., McFarquhar, G.M., Nenes, A., Thornhill, K.L., Wisthaler, A., Zelenyuk, A., and Ziemba L.D.: Aircraft-measured indirect cloud effects from biomass burning smoke in the Arctic and subarctic, Atmos. Chem. Phys. Discuss., 15, 22823–22887, doi:10.5194/acpd-15-22823-2015, 2015, 2015.

Zhao, C. and Garrett, T.J.: Effects of Arctic haze on surface cloud radiative forcing. Geophys. Res. Lett. 10.1002/2014GL062015, 2015.

Table 1. Summary of averaged cloud observations with LWC>0.01 g m^{-3} for study periods 1 and 2. CDNC and LWC without parentheses are referenced to ambient volumes and values in parentheses are referenced to STP. 5;95 are the 5th and 95th percentiles.

Measurement	Period 1 (July 5-11): 35 samples; 1.2 hours in cloud			Period 2 (July 11-21): 27 samples; 0.4 hours in cloud		
	Mean	Median	5;95	Mean	Median	5;95
Altitude (m-msl)	920	178	88;2272	1011	835	97;2608
Temperature (^{o}C)	-1.9	-0.4	-6.5;2.2	+1.2	+2.2	-4.9;3.5
CDNC (STP) (cm^{-3})	75 (85)	93 (91)	1.1;154 (1.1;185)	73 (83)	52 (55)	13;228 (14;265)
LWC (STP) (g m^{-3})	0.12 (0.13)	0.10 (0.12)	0.014;0.32 (0.013;0.32)	0.12 (0.13)	0.12 (0.13)	0.025;0.26 (0.024;0.31)
VMD (µm)	17.2	18.7	9.9;30.0	15.0	14.5	9.1;21.4
CCNC(0.6%) (cm^{-3}): (17 P-1; 27 P-2)	90	120	2;168	81	43	18;227
N50 (cm^{-3})	113	134	4.8;319	126	68	29;334
N100 (cm^{-3})	35	47	1.3;73	81	31	13.8;274
CDNC(STP)/CCNC(0.6%)	0.75	0.56	0.18;1.50	1.18	1.22	0.47;1.87
CDNC(STP)/N50	0.82	0.90	0.16;1.40	0.73	0.68	0.28;1.08
CDNC(STP)/N100	2.78	2.63	0.28;7.94	1.37	1.25	0.58;2.15
CCNC(0.6%)/N50	0.64	0.63	0.50;0.84	0.64	0.64	0.52;0.87
CCNC(0.6%)/N100	1.92	1.79	0.67;3.11	1.27	1.0	0.75;2.28
CO (ppbv)	79	80	77;81	90	87	81;108
LWP (g m^{-2}); (13 P-1; 20 P-2)	30	27	1.5;67	24	18	1.4;75

Table 2. Summary of averaged observations for low-altitude (LA) and higher-altitude (HA) clouds. Values without parentheses are referenced to ambient volumes and values in parentheses are referenced to STP. 5, 95 are the 5th and 95th percentiles.

Measurement	LA (<200m): 24 samples; 0.89 hours in cloud			HA (>200m): 38 samples; 0.72 hours in cloud		
	Mean	Median	5;95	Mean	Median	5;95
Altitude (m-msl)	129	127	79;178	1485	1481	457;2391
Temperature (^{o}C)	+0.6	+0.2	-2.5;2.9	-1.2	+0.9	-6.5;2.7
CDNC (STP) (cm^{-3})	31 (30)	11 (10)	1;106 (1;102)	101 (118)	91 (101)	28;211 (31;245)
LWC (STP) ($g\ m^{-3}$)	0.10 (0.10)	0.05 (0.05)	0.01;0.34 (0.01;0.33)	0.13 (0.15)	0.13 (0.15)	0.04;0.25 (0.04;0.30)
VMD (μm)	20.7	20.1	14.6;31	13.4	12.5	9.1;19.4
CCNC(0.6%) (cm^{-3}); (16 LA; 28 HA)	74	24	2;184	90	58	21;217
N50 (cm^{-3})	91	11	4.2;319	136	133	41;334
N100 (cm^{-3})	26	4	1.3;73	73	47	20;232
CDNC(STP)/CCNC(0.6%)	0.61	0.57	0.18;1.3	1.2	1.2	0.6;1.9
CDNC(STP}/N50	0.61	0.44	0.14;1.5	0.91	0.93	0.5;1.3
CDNC(STP)/N100	2.3	1.4	0.35;9.0	2.1	1.9	0.7;3.7
CCNC(0.6%)/N50	0.66	0.71	0.52;0.7	0.68	0.64	0.5;0.9
CCNC(0.6%)/N100	1.8	1.6	0.96;2.6	1.5	1.1	0.8;3.4
CO (ppbv)	81	80	78;82	86	83	77;107

Figure. Captions

Figure 1. Compilation of the flight tracks. All flights originated from Resolute Bay (74°40'48"N 94°52'12"W).

Figure 2. Satellite images from July 5 when LA clouds were sampled over the two polynyas to the north and from July 8 when LA clouds were sampled along Lancaster Sound (July 8). Lancaster Sound is cloud free on July 5 and mostly covered by cloud on July 8. Resolute Bay is marked with a "X". Images are courtesy of NASA Worldview: https://earthdata.nasa.gov/labs/worldview/.

Figure 3. Four examples of profiles through HA clouds. a) Case from July 7 showing CO, CDNC, CCNC(0.6%) and particle number concentrations, where Nx-100, N100 and N5 are for particles sized between "x" nm and 100 nm, >100 nm and >5 nm respectively. b) Case from July 7 showing LWC, VMD, θ_e and temperature, where VMD, θ_e and temperature have been scaled as indicated in the legend. c) As in a), but case from July 17 and without N5. d) As in b), but case from July 17. e) As in a), but case from July 19. f) As in b) but case from July 19. g) As in a) but case from July 20 and without N5. H) as in b), but case from July 20. The CDNC are all referenced to STP, and θ_e is given in degrees Centigrade before scaling.

Figure 4. Time series during the sampling of low (LA) cloud or fog over the polynyas north of Resolute Bay. a) July 5 time series showing CO, CDNC, CCNC(0.6%) and particle number concentrations, where N30-100 is for particles sized between 30 nm and 100 nm and N100 is for particles sized >100 nm. b) July 7 time series showing CO, CDNC and particle number concentrations, where N20-100, N50-100 and N100 are for particles sized between 20 nm and 100 nm, between 50 nm and 100 nm and >100 nm respectively. CCNC(0.6%) measurements are unavailable for this period on July 7. Wind direction and relative position of polynyas are indicated in both panels. CDNC are referenced to STP.

Figure 5. Time series of altitude, CO, N80-100, N90-100, N100, CCNC(0.6%) and CDNC from low cloud (LA) cloud sampling over Lancaster Sound on July 8. The cloud was deeper over the open water of the Sound (see satellite picture in Fig. 2b). Over the ice to the west, the cloud was not as deep and could not be sampled. Segments over water and ice are indicated at the top of the figure.

Figure 6. Profiles down into cloud showing a) θ_e, b) LWC and c) VMDData for periods 17:27-17:29 UT and 17:38-17:39 UT during July 8. d) shows CDNC, N100, CO and CCNC(0.6%) for the 17:27-17:29 UT profile, and e) shows CDNC, N100, CO and CCNC(0.6%) for the 17:38-17:39 UT profile.

Figure 7. The LWC plotted as a function of the CDNC (a) and VMD (b) for the LA (orange) and HA (blue) samples. Linear regressions for each of the LA and HA samples are also plotted, and the coefficients of determination are given in the legends.

Figure 8. Plots of CDNC versus a) N100 and b) N50. Points are identified between LA (yellow) and HA (blue) samples, and the 1:1 lines are for reference.

Figure 9. a) CDNC plotted versus the CCNC(0.6%) measured at 0.6% supersaturation; points are identified between LA (yellow) and HA (blue) samples, and linear regressions through the origin are shown. b) CCNC(0.6%) plotted versus N50 and N100; power law fits to each are provided for reference.

Figure 10. The mean VMD of all cloud samples plotted versus the CDNC. All CDNC are referenced to the in-situ pressure. The dashed vertical green line represents the "CCN-limited" division discussed by Mauritsen et al (2011) and estimated here as 16 cm^{-3}. The solid black line is another reference showing the relationship between VMD and CDNC for a constant LWC: the study mean LWC of 0.12 g m^{-3} (Table 1). Samples with higher CO (>90 ppbv) are identified by the open red circles. Also highlighted for the discussion are LA samples from July 5 (red dots) and July 7 (orange dots). The median CDNC are 1.3 cm^{-3} and 7.8 cm^{-3}, for July 5 and 7, respectively; the N50 are 6 cm^{-3} and 8.3 cm^{-3} for July 5 and 7, respectively; the N100 are 3 cm^{-3} and 2.2 cm^{-3} for July 5 and July 7, respectively.

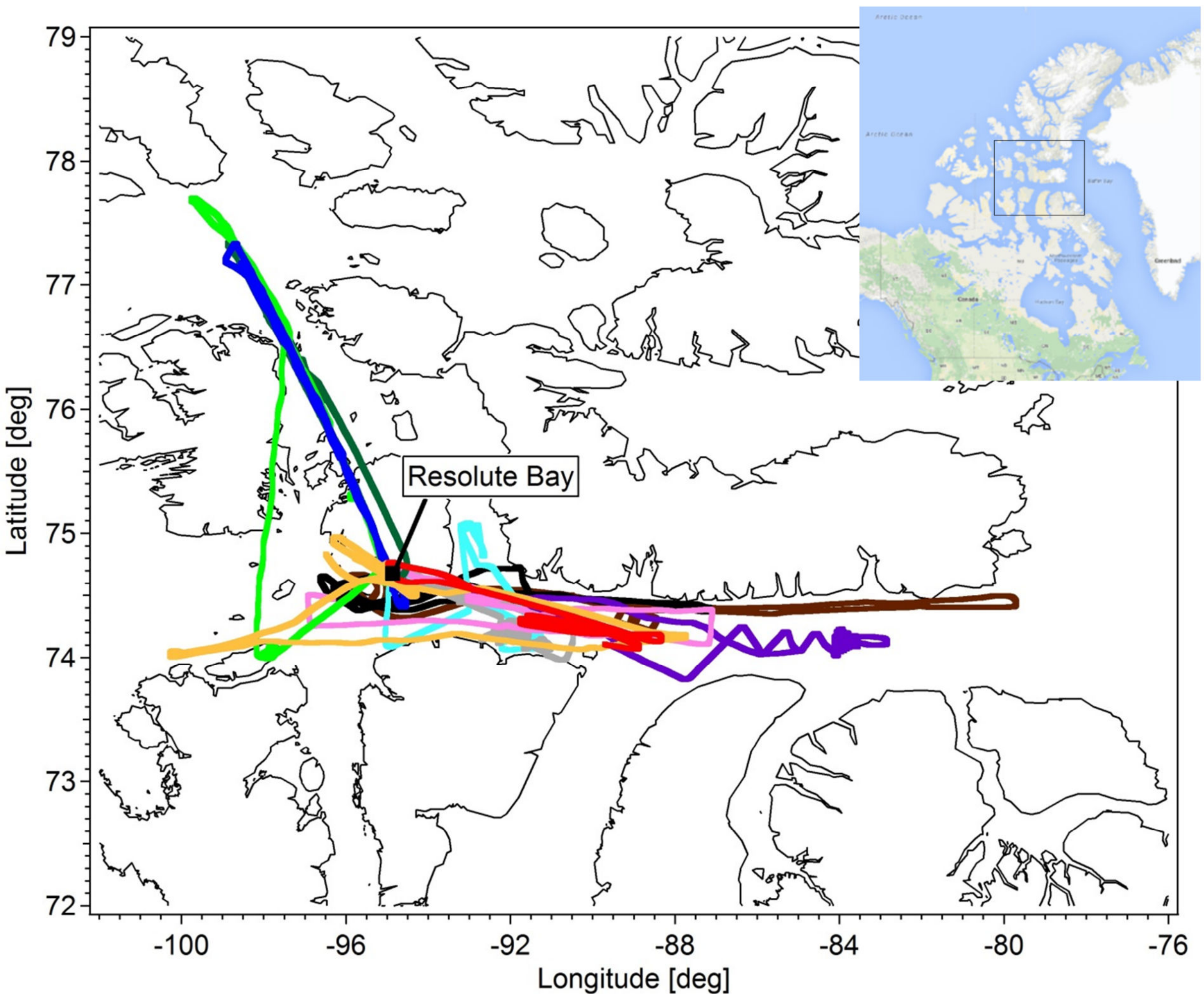

Figure 1. Compilation of the flight tracks. All flights originated from Resolute Bay (74°40'48"N 94°52'12"W).

July 5, 2014 July 8, 2014

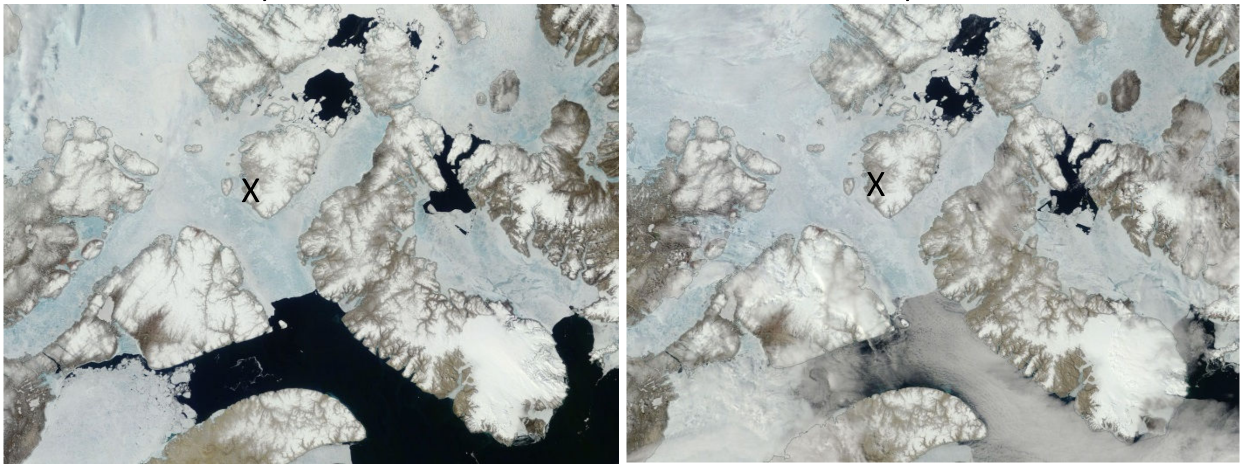

Figure 2. Satellite images from July 5 when LA clouds were sampled over the two polynyas to the north and from July 8 when LA clouds were sampled along Lancaster Sound (July 8). Lancaster Sound is cloud free on July 5 and mostly covered by cloud on July 8. Resolute Bay is marked with a “X”. Images are courtesy of NASA Worldview: https://earthdata.nasa.gov/labs/worldview/.

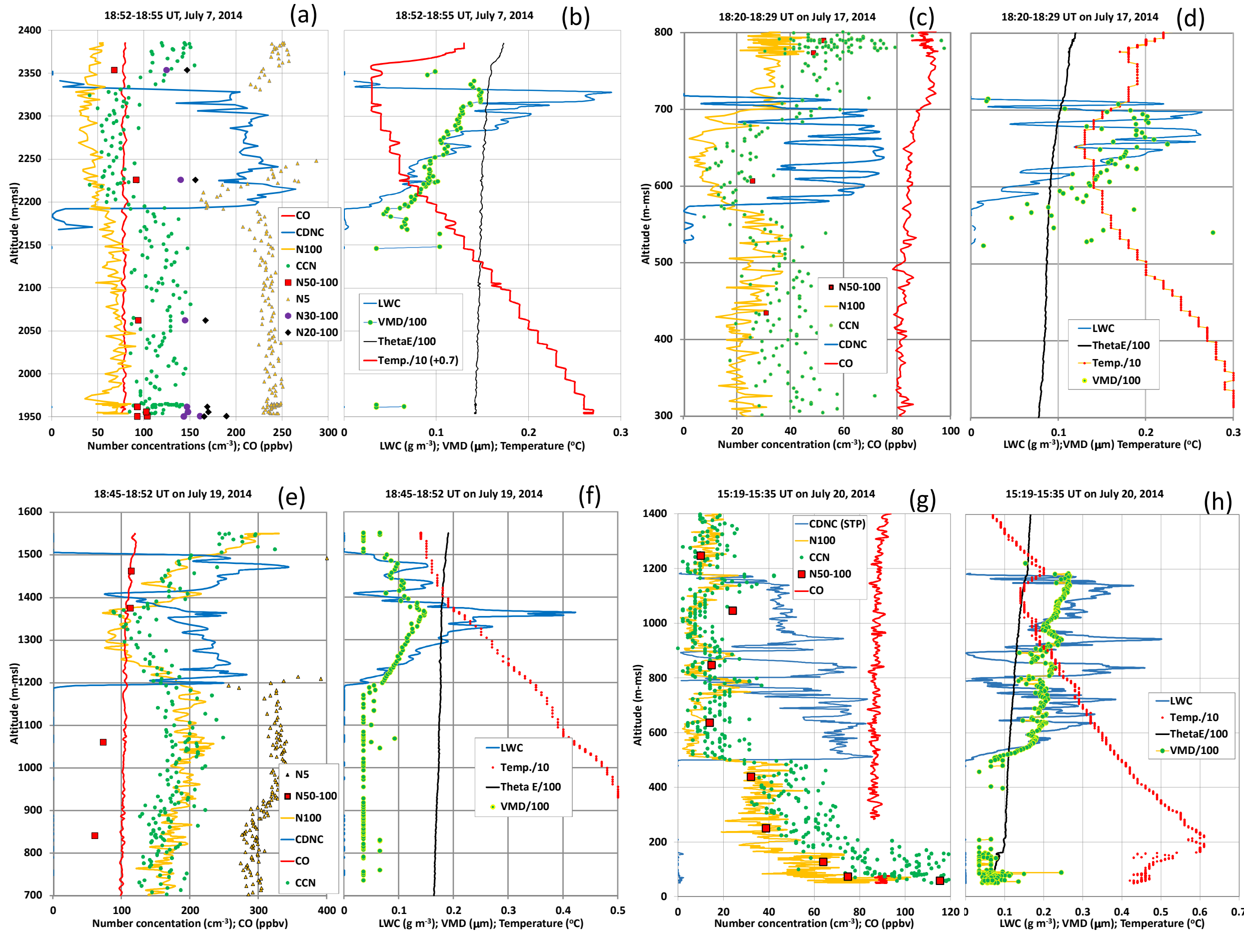

Figure 3. Four examples of profiles through HA clouds. a) Case from July 7 showing CO, CDNC, CCNC(0.6%) and particle number concentrations, where Nx-100, N100 and N5 are for particles sized between “x” nm and 100 nm, >100 nm and >5 nm respectively. b) Case from July 7 showing LWC, VMD, θ_e and temperature, where VMD, θ_e and temperature have been scaled as indicated in the legend. c) As in a), but case from July 17 and without N5. d) As in b), but case from July 17. e) As in a), but case from July 19. f) As in b) but case from July 19. g) As in a) but case from July 20 and without N5. H) as in b), but case from July 20. The CDNC are all referenced to STP, and θ_e is given in degrees Centigrade before scaling.

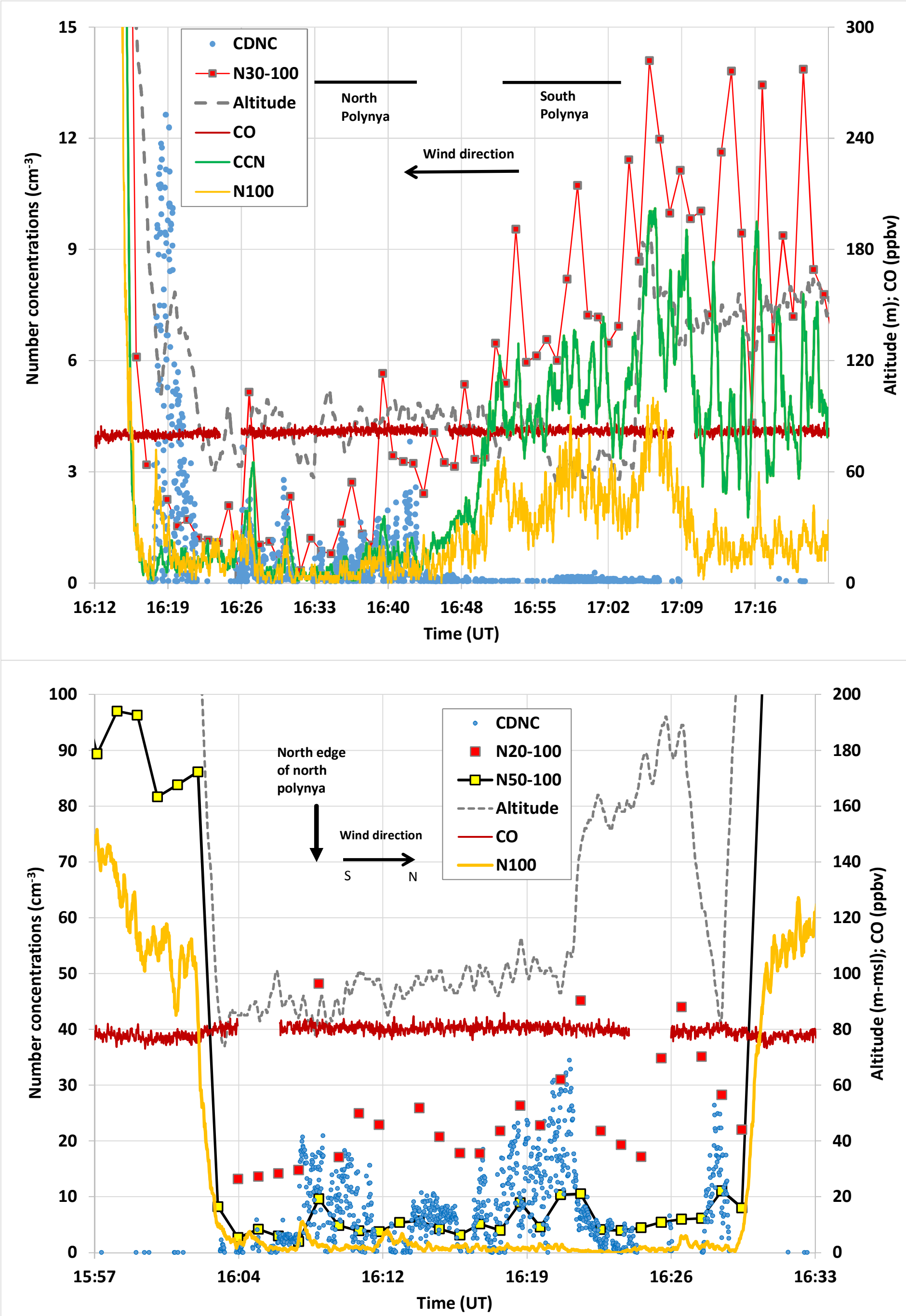

Figure 4. Time series during the sampling of low (LA) cloud or fog over the polynyas north of Resolute Bay. a) July 5 time series showing CO, CDNC, CCNC(0.6%) and particle number concentrations, where N30-100 is for particles sized between 30 nm and 100 nm and N100 is for particles sized >100 nm. b) July 7 time series showing CO, CDNC and particle number concentrations, where N20-100, N50-100 and N100 are for particles sized between 20 nm and 100 nm, between 50 nm and 100 nm and >100 nm respectively. CCNC(0.6%) measurements are unavailable for this period on July 7. Wind direction and relative position of polynyas are indicated in both panels. CDNC are referenced to STP.

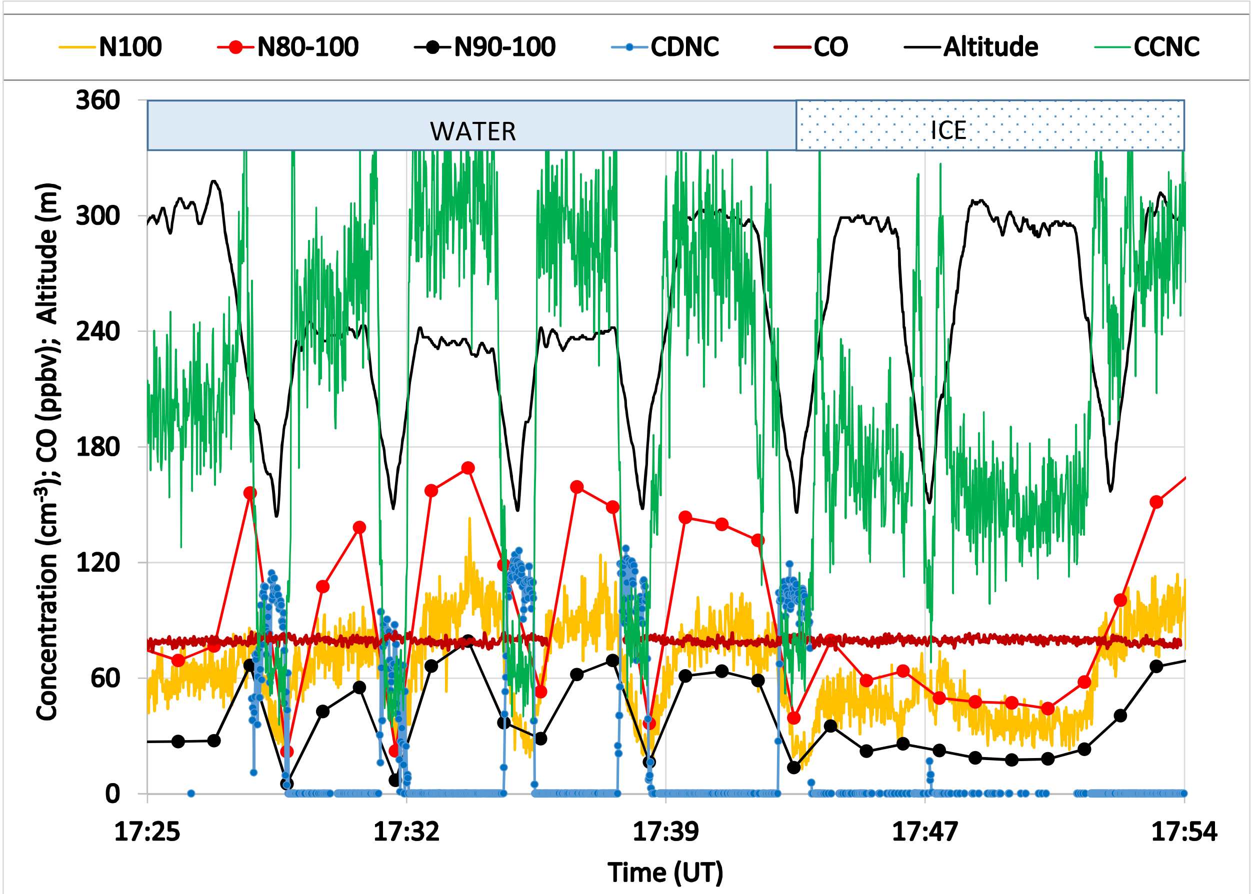

Figure 5. Time series of altitude, CO, N80-100, N90-100, N100, CCNC(0.6%) and CDNC from low cloud (LA) cloud sampling over Lancaster Sound on July 8. The cloud was deeper over the open water of the Sound (see satellite picture in Fig. 2b). Over the ice to the west, the cloud was not as deep and could not be sampled. Segments over water and ice are indicated at the top of the figure.

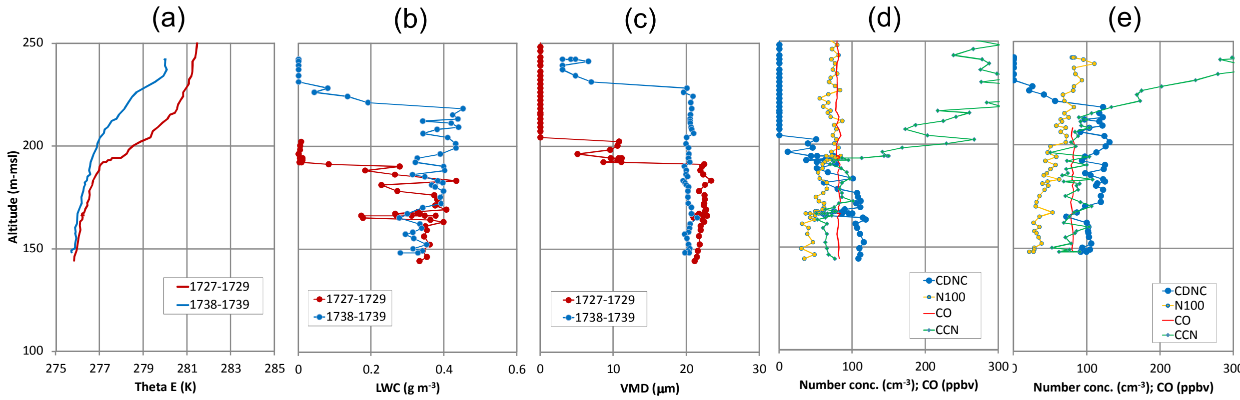

Figure 6. Profiles down into cloud showing a) θe, b) LWC and c) VMDData for periods 17:27-17:29 UT and 17:38-17:39 UT during July 8. d) shows CDNC, N100, CO and CCNC(0.6%) for the 17:27-17:29 UT profile, and e) shows CDNC, N100, CO and CCNC(0.6%) for the 17:38-17:39 UT profile.

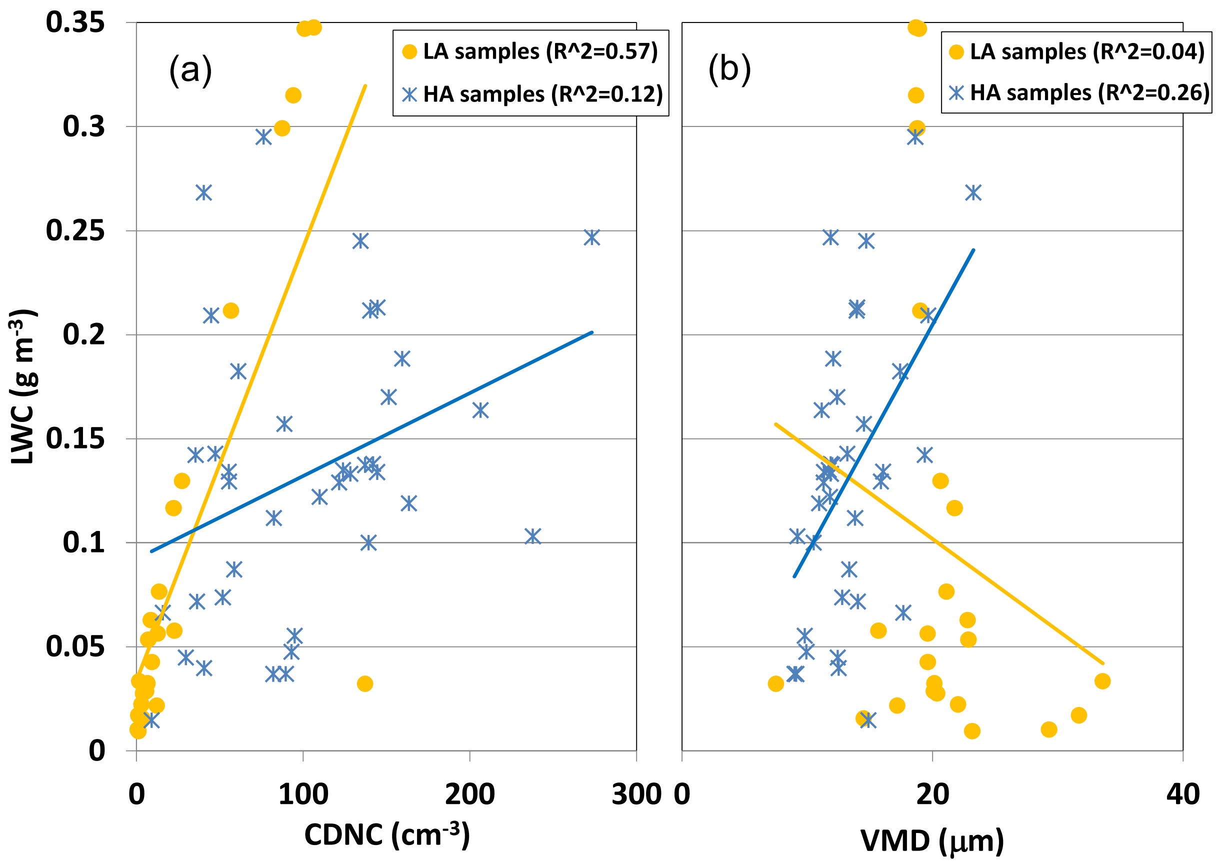

Figure 7. The LWC plotted as a function of the CDNC (a) and VMD (b) for the LA (orange) and HA (blue) samples. Linear regressions for each of the LA and HA samples are also plotted, and the coefficients of determination are given in the legends.

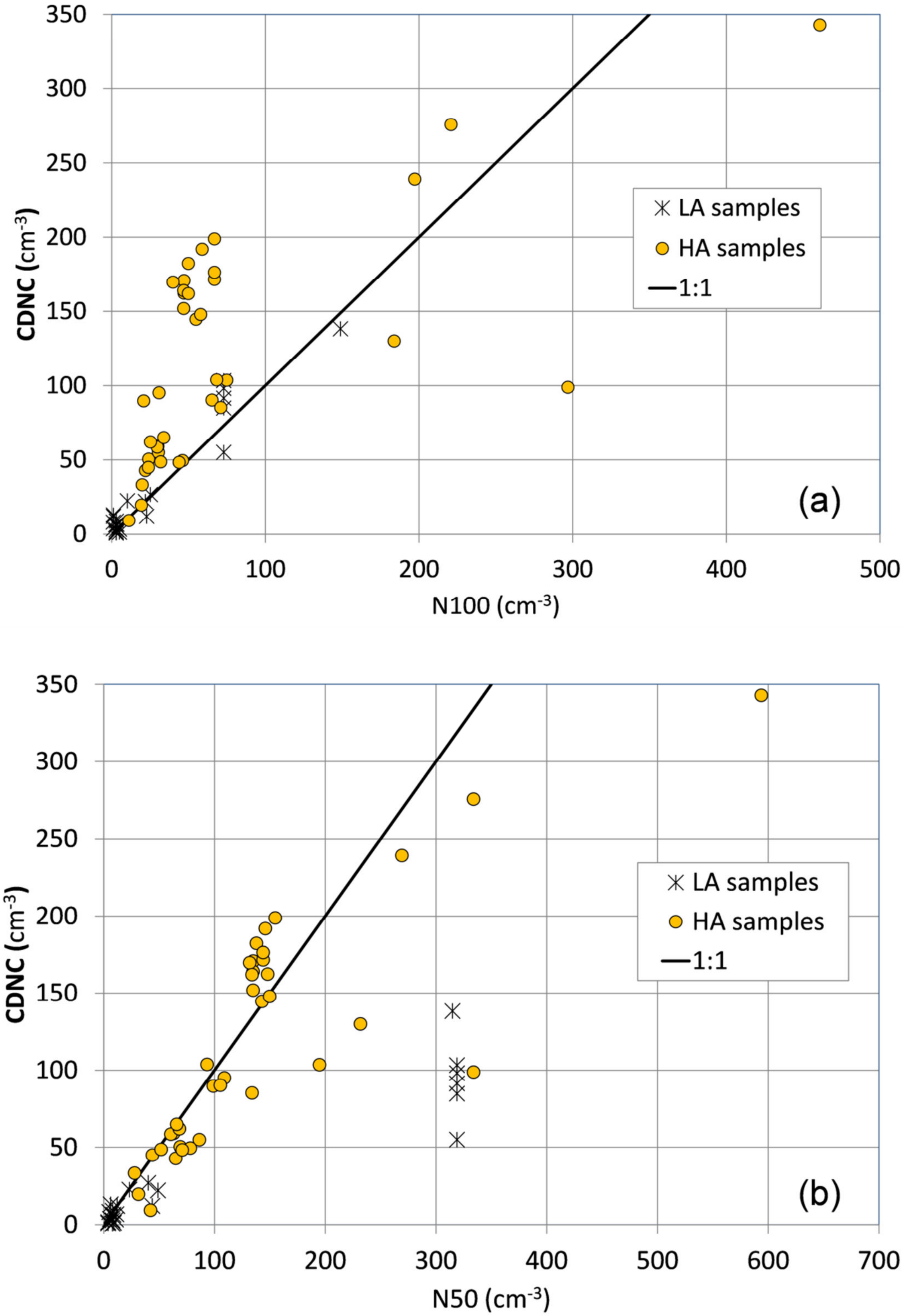

Figure 8. Plots of CDNC versus a) N100 and b) N50. Points are identified between LA (yellow) and HA (black asterisk) samples, and the 1:1 lines are for reference.

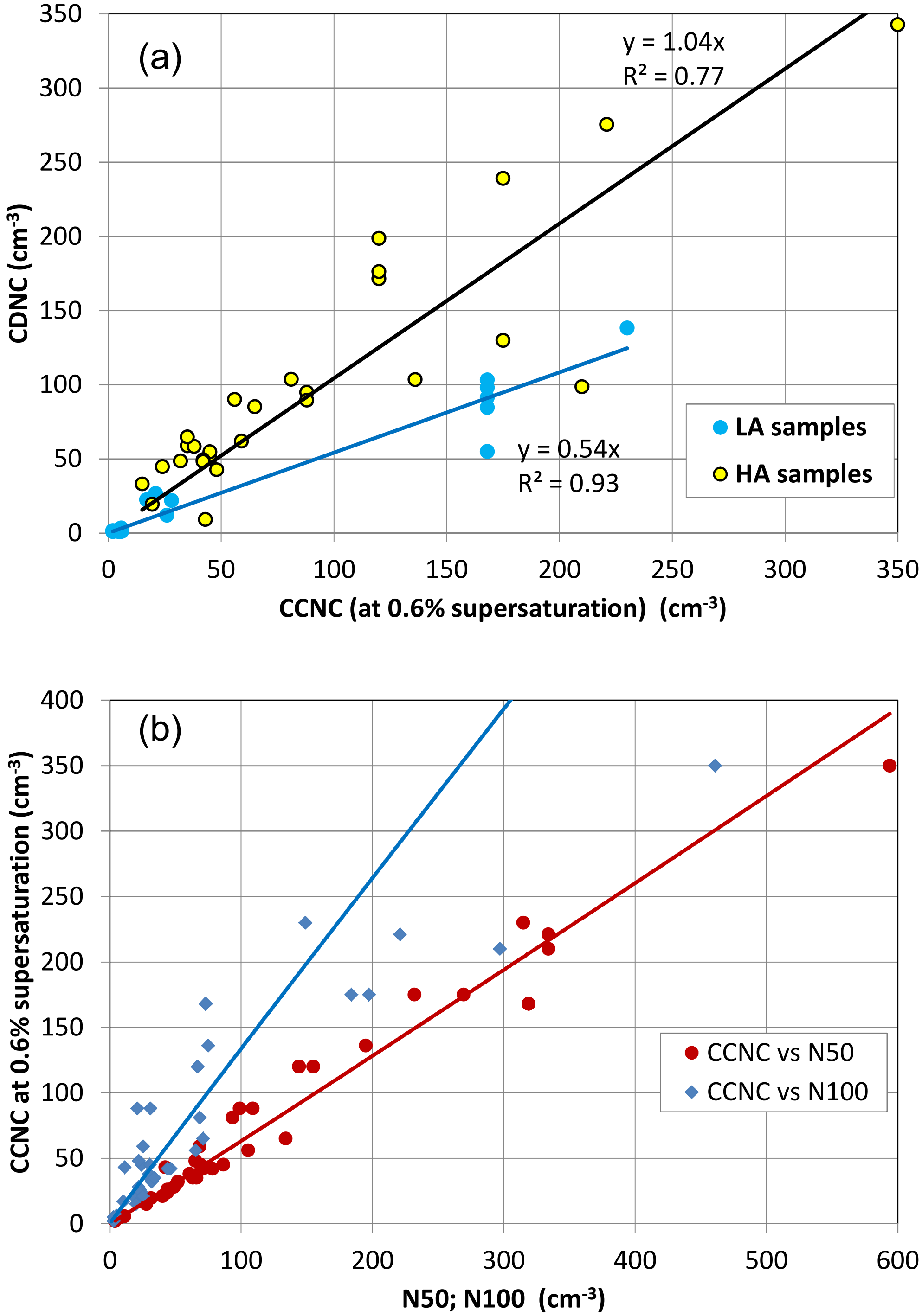

Figure 9. a) CDNC plotted versus the CCNC measured at 0.6% supersaturation; points are identified between LA (yellow) and HA (blue) samples, and linear regressions through the origin are shown; the CCNC(0.6%) points are limited to 44 of the 62 total, due to problems with the CCN measurement; the 44 are split 16 and 28 between LA and HA,. b) CCNC(0.6%) (44 points) plotted versus N50 and N100; power law fits to each are provided for reference.

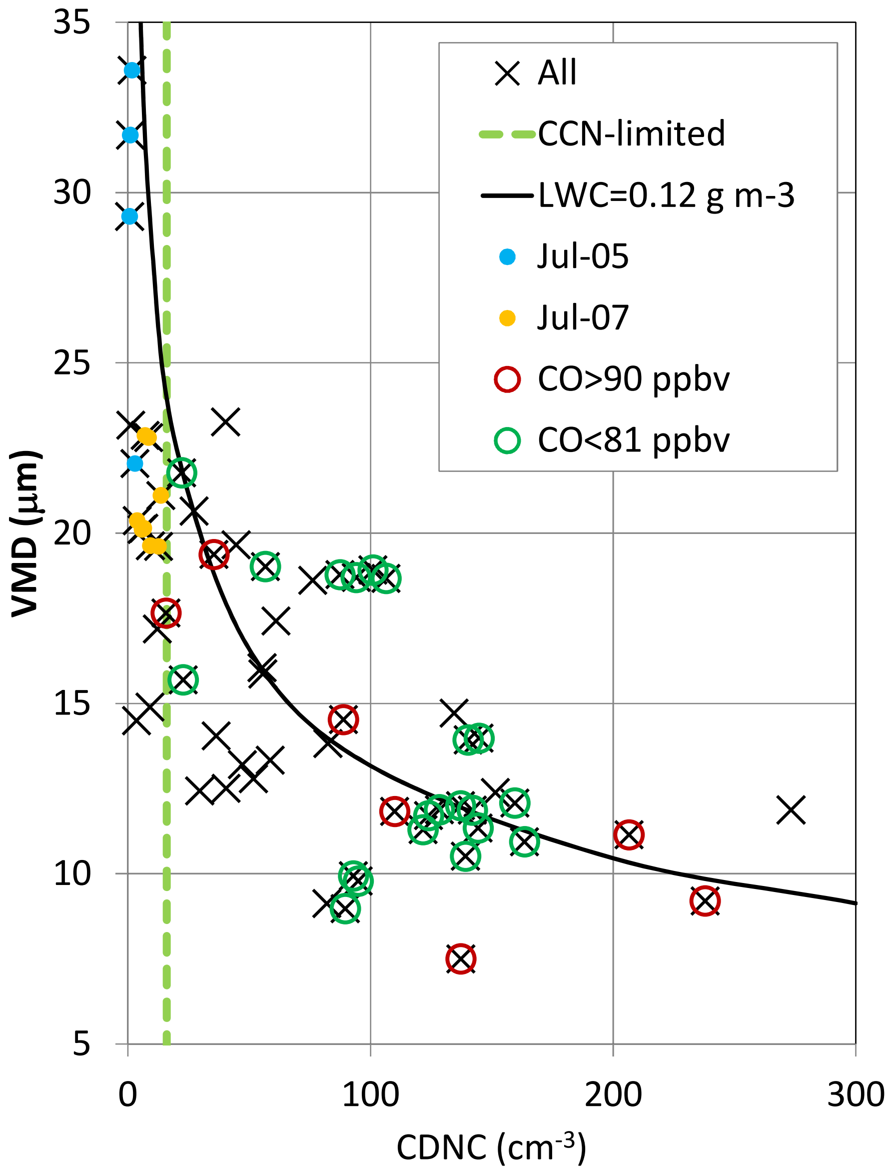

Figure 10. The mean VMD of all cloud samples plotted versus the CDNC. All CDNC are referenced to the ambient pressure. The dashed vertical green line represents the "CCN-limited" division discussed by Mauritsen et al (2011) and estimated here as 16 cm^{-3}. The solid black line is another reference showing the relationship between VMD and CDNC for a constant LWC: the study mean LWC of 0.12 g m^{-3} (Table 1). Samples with higher CO (>90 ppbv) are identified by the open red circles. Also highlighted for the discussion are LA samples from July 5 (blue dots) and July 7 (orange dots).